JOURNAL OF NATURAL PRODUCTS

Review

Cite This: J. Nat. Prod. 2018, 81, 703−721

pubs.acs.org/jnp

Quest for Efficacious Next-Generation Taxoid Anticancer Agents and Their Tumor-Targeted Delivery

Iwao Ojima,* Xin Wang, Yunrong Jing, and Changwei Wang

Department of Chemistry and Institute of Chemical Biology & Drug Discovery, Stony Brook University−State University of New York, Stony Brook, New York 11794-3400, United States

ABSTRACT: Paclitaxel and docetaxel are among the most widely used chemotherapeutic drugs against various types of cancer. However, these drugs cause undesirable side effects as well as drug resistance. Therefore, it is essential to develop next-generation taxoid anticancer agents with better pharmacological properties and improved activity especially against drug-resistant and metastatic cancers. The SAR studies by the authors have led to the development of numerous highly potent novel second- and third-generation taxoids with systematic modifications at the C-2, C-10, and C-3′ positions. The third-generation taxoids showed virtually no difference in potency against drug-resistant and drug-sensitive cell lines. Some of the next-generation taxoids also exhibited excellent potency against cancer stem cells. This account summarizes concisely investigations into taxoids over 25 years based on a strong quest for the discovery and development of efficacious next-generation taxoids. Discussed herein are SAR studies on different types of taxoids, a common pharmacophore proposal for microtubule-stabilizing anticancer agents and its interesting history, the identification of the paclitaxel binding site and its bioactive conformation, characteristics of the next-generation taxoids in cancer cell biology, including new aspects of their mechanism of action, and the highly efficacious tumor-targeted drug delivery of potent next-generation taxoids.

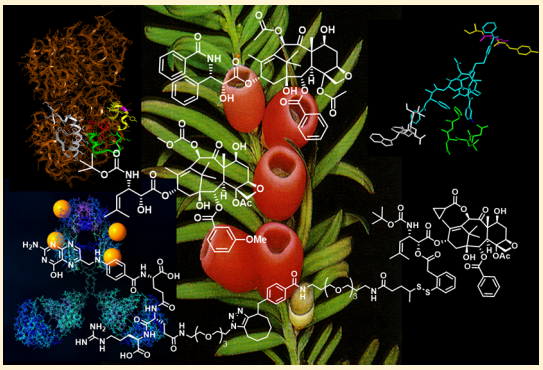

INTRODUCTION

One of the authors (I.O.) has had the pleasure of collaborating with Professor Susan Band Horwitz for the last quarter century on various aspects of the chemistry and biology of taxol (paclitaxel), docetaxel, and other taxoids (Figure 1). Therefore,

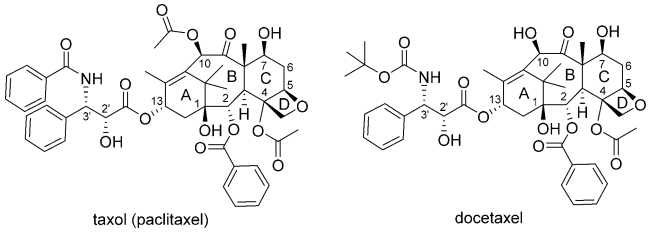

Figure 1. Taxol (paclitaxel) and docetaxel.

the authors believe that it is appropriate to summarize our endeavor driven by the quest for efficacious next-generation taxoid anticancer agents, featuring our collaboration with Dr. Horwitz and findings in perspective as a review article, including relevant results from other research laboratories.

Throughout our medicinal chemistry and drug discovery efforts, focusing on next-generation taxoids derived from 10-deacetylbaccatin III (10-DAB), 14β-hydroxy-10-deacetylbaccatin III (14β-OH-DAB), *C-seco*-baccatin, and analogues with fluorinated C13-isoserine side chains, Dr. Horwitz has helped us identify characteristic effects of these taxoids on tubulin and its microtubule formation, as compared to those of guanosine triphosphate (GTP) and paclitaxel. These studies led us to investigate the nature of the formed microtubules in detail, as well as the thermodynamic basis for interactions with tubulin/microtubules. We had intensive collaborations on the identification of the taxol-binding site in tubulin monomers, as well as P-glycoprotein (Pgp) by designing, synthesizing, and using radio- and photoaffinity-labeled taxol derivatives. We also collaborated on the proposal of a possible common pharmacophore for several naturally occurring microtubule-stabilizing agents with diverse structures, prior to the structural information on tubulin-bound structures of paclitaxel and epothione A by cryo-electron microscopy (cryo-EM) of a zinc-stabilized α,β-tubulin dimer model became available. Then, with this cryo-EM data for the taxol−tubulin complex model structure in hand, we succeeded in identifying a single amino acid residue (Arg282) in β-tubulin by using a radio- and photoaffinity-labeled taxol derivative. This led us to investigate the bioactive structure (conformation) of taxol by solid-state NMR spectroscopy of taxol-bound microtubules and computer modeling. Our strategy for the discovery and development of next-generation taxoids had a very clear focus on their activities against multidrug-resistant (MDR) cancer cell lines and tumors

Special Issue: Special Issue in Honor of Susan Horwitz

Received: December 1, 2017
Published: February 22, 2018

DOI: 10.1021/acs.jnatprod.7b01012
J. Nat. Prod. 2018, 81, 703−721

expressing MDR phenotypes, especially, Pgp. Dr. Horwitz had a keen interest in all kinds of taxane resistance,[1] not limited to Pgp-based resistance. Her pioneering work on the overexpression of class III β-tubulin (βIII-tubulin) as a possible cause of taxol-resistance based on the analysis of clinical samples inspired extensive studies on this particular type of drug resistance and its solution by discovering compounds that could overcome it. We have investigated the activities of next-generation taxoids, including *C-seco*-taxoids, and found highly potent taxoids that can overcome drug resistance based on βIII-tubulin overexpression.

Building upon the discovery and development of highly potent next-generation taxoids, especially against drug-resistant cancer cells and tumors, we initiated an investigation into tumor-targeted drug delivery of these taxoids. We constructed various drug conjugates, bearing mechanism-based smart linkers and a variety of tumor-targeting molecules, using nanoscale vehicles that could exploit enhanced permeability and retention (EPR) effects, that are selective to tumors. We have also found that next-generation taxoids possess high potency and efficacy against cancer stem cells (CSCs) and CSC-initiated tumors. More recently, we have found that some of the next-generation taxoids exert efficacy through mechanisms of action (MOAs) that have not been observed for taxol and docetaxel.

Accordingly, drug discovery based on taxoids is still active and thriving after a quarter of a century since the U.S. FDA approval of taxol in 1992. This account will concisely go through the rich history of taxoid research on different fronts in perspective.

DISCOVERY AND DEVELOPMENT OF NEXT-GENERATION TAXOIDS BASED ON STRUCTURE–ACTIVITY (SAR) STUDIES

Paclitaxel and docetaxel are among the most widely used chemotherapeutic drugs against various types of cancers.[2] Another taxane anticancer drug, cabazitaxel, was recently approved by the FDA as a combination therapy for prostate cancer treatment.[3] Despite their potent antitumor activity, paclitaxel and docetaxel cause undesirable side effects as well as drug resistance.[2] Thus, it was apparent in the early 1990s that it would be essential to develop new taxane anticancer agents with fewer side effects, enhanced activity against multidrug-resistant human tumors, and superior pharmacological properties. The limited availability of these two drugs, as well as the pursuit for improved analogues, made them the focus of many synthetic investigations and extensive SAR studies.[4−7] For securing the supply of taxol through practical semisynthesis, a major breakthrough was the isolation of 10-deactylbaccatin III (10-DAB) (Figure 2) from the needles and leaves of the European yew, *Taxus baccata*, by Potier's group in the early 1980s.[8,9]

Initial SAR studies of paclitaxel were primarily performed by the laboratories of Kingston and Potier in the 1980s to the early early 1990s.[10−13] These studies of taxol guided the site-specific modifications of this unique tetracyclic diterpene skeleton. For SAR studies of taxoids from the early 1990s until now, in the vast majority of cases, the β-lactam synthon method, i.e., the asymmetric synthesis of a C-13-isoserine synthon (β-lactam)[14−17] combined with a highly efficient ring-opening coupling, has been used. The ring-opening coupling protocol, "Ojima–Holton coupling", was invented independently by Dr. Robert Holton (Florida State University, Tallahassee)[18,19] and our laboratory.[15−17] The β-lactam synthon method enabled a practical semisynthesis of paclitaxel, used in several total syntheses of paclitaxel, and provided a highly efficient method for the synthesis of a variety of taxoids for medicinal chemistry and drug discovery (Figure 2).[20]

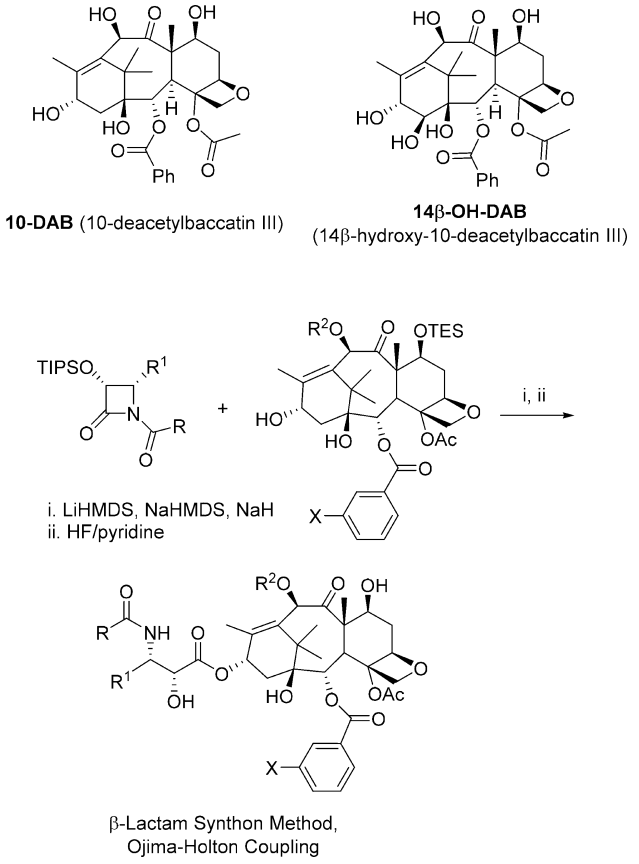

Figure 2. 10-DAB, 14β-OH-10-DAB, and the β-lactam synthon method.

Second- and Third-Generation Taxoids Derived from 10-Deacetylbaccatin III. Our SAR study on taxoids has indicated that (i) the C-3′-phenyl group can be replaced with an alkenyl or alkyl group and (ii) the C-10 position can be modified with certain acyl groups that make the compounds 1–2 orders of magnitude more potent than paclitaxel and docetaxel against MDR human cancer cell lines. These highly potent taxoids were termed "second-generation taxoids".[21,22] Following the discovery of the beneficial effect of *meta* substitution on the C-2-benzoyl group of paclitaxel by the group of Dr. David Kingston (Virginia Tech, Blacksburg),[23,24] we found that similar substitution (e.g., MeO, N_3, Cl, F, etc.) at the *meta* position of the C-2-benzoyl group of the second-generation taxoids enhanced their potencies up to 3 orders of magnitude over those of the parent drugs against MDR human cancer cell lines, wherein drug resistance was virtually resolved.[22,25,26] Thus, those taxoids were termed "third-generation taxoids".[27] General structures of these second- and third-generation taxoids, i.e., "next-generation taxoids", developed in our laboratory are shown in Figure 3. It is worth mentioning that these next-generation taxoids can overcome not only MDR by overexpression of Pgp[22] but also other taxane-resistance mechanisms such as the resistance caused by overexpression of βIII-tubulin[28] and point mutations at the taxane binding site[22] in microtubules.

DOI: 10.1021/acs.jnatprod.7b01012
J. Nat. Prod. 2018, 81, 703−721

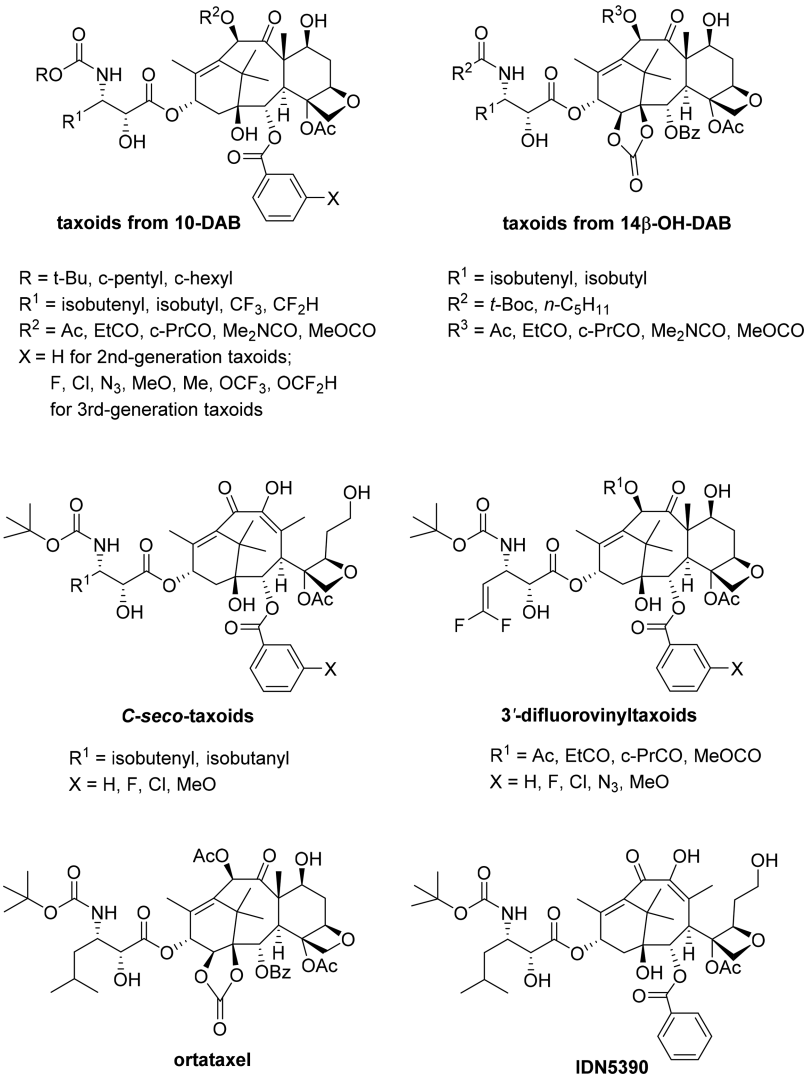

Figure 3. Structures of next-generation taxoids.

Taxoids Derived from 14*β*-Hydroxybaccatin III. 14*β*-Hydroxy-10-deacetylbaccatin III (14*β*-OH-DAB, Figure 2) was isolated from the needles of *Taxus wallichiana* Zucc.[29] As this natural product was more water-soluble than 10-DAB, the corresponding taxoids were expected to have better bioavailability and diminished hydrophobicity-related drug resistance. Thus, derivatives of docetaxel, as well as second-generation taxoids based on this unique baccatin derivative, were synthesized and their biological activities examined.[30] Also, a series of second-generation taxoids, bearing a 1,14-carbonate of 14*β*-OH-DAB, were synthesized and their biological activities evaluated (Figure 3).[31] Most of these novel taxoids showed better activity against drug-sensitive cancer cell lines with 1 order of magnitude higher potency against an MDR cancer cell line.[31] After extensive preclinical evaluations, one of these taxoids, ortataxel (Figure 3), was selected as a clinical candidate and advanced to phase II clinical trials.[32]

***C-seco*-Taxoids.** *C-seco*-taxoid IDN5390, synthesized from *C-seco*-baccatin III, exhibited 8 times higher potency than paclitaxel against a drug-resistant OVCAR3 ovarian cancer cell line, as well as the taxane-resistant ovarian cancer cell lines A2780TC1 and A2780TC3.[33] To explore the unique activity of *C-seco*-taxoids against cancer cell lines overexpressing *β*III-tubulin, a series of *C-seco*-taxoids, bearing modifications at the C-2 and C-3′ positions, were synthesized, and their potencies examined (Figure 3).[34] These *C-seco*-taxoids did not show cross-resistance to cisplatin-resistant A2780CIS and topotecan-resistant A2780TOP cell lines and showed remarkably higher potency than paclitaxel against the paclitaxel-resistant A2780TC1 and A2780TC3 cell lines, overexpressing *β*III-tubulin.[34]

3′-Difluorovinyltaxoids. As a part of the systematic design and development of the next-generation taxoids, we investigated novel 3′-trifluoromethyl- and 3′-difluoromethyltaxoids with C-10 as well as C-10/C-2 modifications.[35−37] Thus, it was shown that trifluoromethyl and difluoromethyl groups are viable modifiers of the C-3′ position, and a number of highly potent fluorotaxoids were identified. Nevertheless, the isobutenyl group was found to be the best substituent at C-3′ for cytotoxicity. However, our study on the metabolic stability of 3′-isobutyl- and 3′-isobutenyltaxoids revealed a marked difference in metabolism between the next-generation taxoids and those of docetaxel and paclitaxel.[38] The metabolism study showed that CYP 3A4 in the cytochrome P450 family in humans metabolized these taxoids, such as SB-T-1214 (**1**) and SB-T-1216 (**2**), through hydroxylation primarily at the two allylic methyl groups of the C-3′-isobutenyl group (Figure 4).[38]

DOI: 10.1021/acs.jnatprod.7b01012
J. Nat. Prod. 2018, 81, 703−721

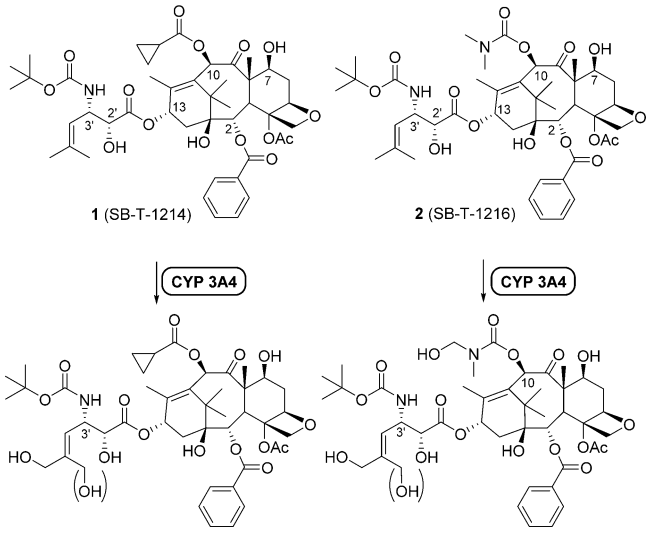

Figure 4. Primary sites of hydroxylation on the next-generation taxoids by the P450 family of enzymes.

In order to prevent this allylic hydroxylation, we introduced a difluorovinyl group by mimicking the 3′-isobutenyl group.[39] A series of novel 3′-difluorovinyltaxoids were synthesized through the Ojima–Holton coupling of enantiopure (3*R*,4*R*)-4-difluorovinyl-*β*-lactam with various baccatins with modifications at the 10 and/or 2 positions.[39]

3′-Difluorovinyltaxoids exhibit impressive potencies against human breast, ovarian, colon, and pancreactic cancer cell lines.[39] It has also been shown that these fluorotaxoids initiate apoptosis primarily via the activation of caspases 2, 8, and 9.[40] 3′-Difluorovinyltaxoids exhibited 1–2 orders of magnitude better potency against MCF-7 breast, HCT-29 colon, and PANC-1 pancreatic cancer cell lines (drug-sensitive) and 2–3 orders of magnitude higher potency against the NCI/ADR cancer cell line (drug-resistant) than that of paclitaxel.[39]

COMMON PHARMACOPHORE HYPOTHESIS FOR MICROTUBULE-STABILIZING ANTICANCER AGENTS

Paclitaxel was the first naturally occurring microtubule-stabilizing anticancer agent (MSAA), which was characterized mechanistically by Dr. Susan Band Horwitz.[41] Following this discovery, several other natural products, such as epothilones A and B (**3a**, **3b**),[42] eleutherobin (**4**),[43] discodermolide (**5**),[44] and (−)-zampanolide (**7**),[45] which were isolated from myxobacterium, coral, and marine sponges (Figure 5), have also been identified as MSAAs.[41,46] Although these natural products possess diverse structures, their activities are comparable to or better than those of paclitaxel in various assays.[43,44,47–49] Moreover, these compounds were found to competitively inhibit the binding of [^{3}H]-paclitaxel,[47,50–52] which strongly suggests the existence of a common or at least closely overlapping binding site in microtubules.

Common Pharmacophore Proposal for Microtubule-Stabilizing Anticancer Agents. In collaboration with Dr. Horwitz and Dr. Samuel Danishefsky (Memorial Sloan-Kettering Cancer Center, New York), we proposed a possible common pharmacophore for paclitaxel, epothilones A and B (**3a** and **3b**), eleutherobin (**4**), and discodermolide (**5**) based on the conformational analysis of a totally nonaromatic and active taxoid, nonataxel (**6**).[50] Since the phenyl rings in paclitaxel and docetaxel were generally considered essential for their potent cytotoxicity at that time, the discovery of highly potent totally nonaromatic taxoids, represented by **6**, was a surprise to the field. Nonataxel (**6**) exhibited subnanomolar IC_{50} values against MCF7 human breast (0.9 nM), A121 human ovarian (0.9 nM), and A549 human non-small-cell lung (0.9 nM) cancer cell lines and was more potent than paclitaxel and docetaxel.[50] In the absence of credible protein-bound MSAA structures at that time, the useful information we had on hand was the crystal structures of docetaxel and paclitaxel, as well as their structures (conformations) in protic and nonprotic solvent systems.[5,53–55] On the basis of detailed 2D NMR studies on the conformation of nonataxel in DMSO/water in combination with computational modeling, we determined a plausible 3D structure of **6** and searched computationally for

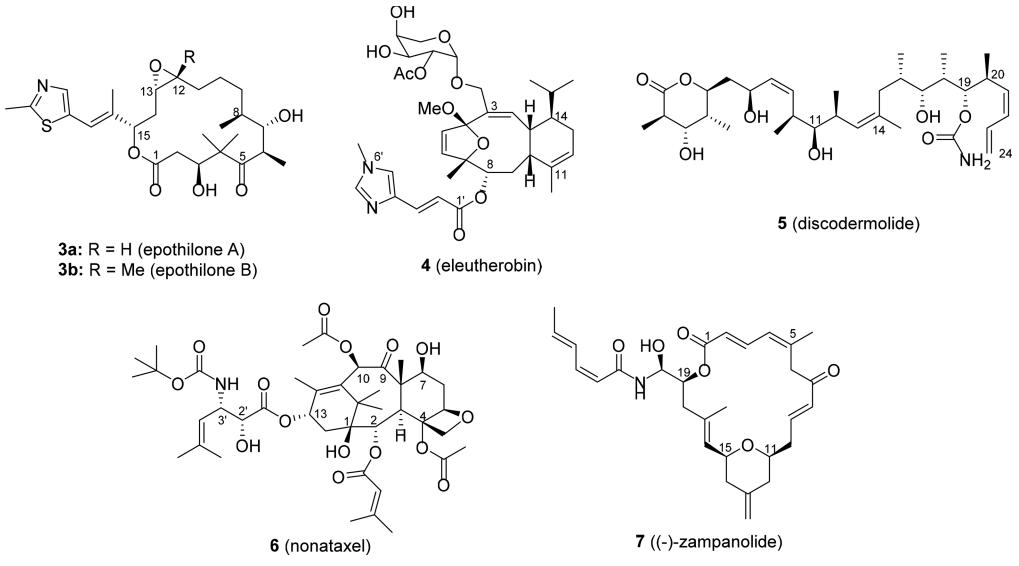

Figure 5. Various naturally occurring microtubule-stabilizing agents and nonataxel (**6**).

DOI: 10.1021/acs.jnatprod.7b01012
J. Nat. Prod. 2018, 81, 703–721

the best overlays with **3b**, **4**, and **5**. This operation produced "looks very good" overlays, as shown in Figure 6. These overlay

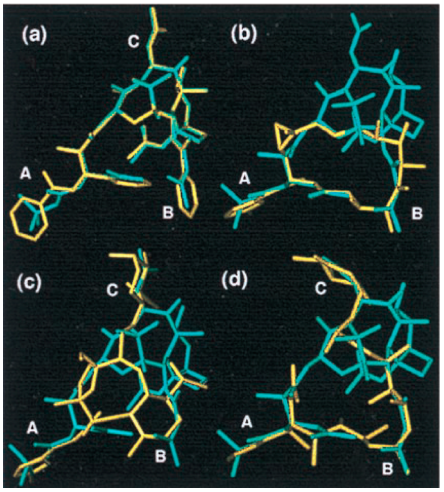

Figure 6. Overlay of nonataxel (**6**, cyan) with (a) paclitaxel, (b) epothilone B (**3b**), (c) eleutherobin (**4**), and (d) discodermolide (**5**) (all in yellow). Designators A, B, and C correspond to regions of common overlap. Adapted from ref 50 with permission.

structures for the proposed common pharmacophore also explained the SAR study results for **3**, **4**, and sarcodictyns (eleutherobin without a sugar side chain).[50] In addition, a macrocyclic hybrid of paclitaxel, docetaxel, and nonataxel (**6**), SB-TE-1120 (**8**) (Figure 7), was designed and synthesized,

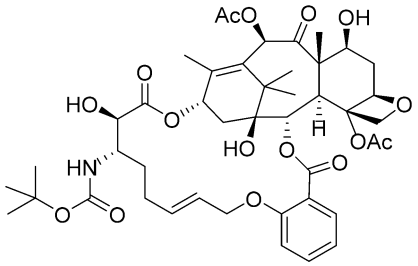

8 (SB-TE-1120)

Figure 7. Macrocyclic hybrid taxoid.

which exhibited moderate cytotoxicity (IC_{50} 0.39 μM) against the MDA-435/LCC6-WT human breast cancer cell line and 37% activity as compared to paclitaxel in the tubulin polymerization assay.[50] Although macrocyclic hybrid molecules, additionally synthesized, did not exceed the potency of **8**, their syntheses proved the power of Ru-catalyzed ring-closing metathesis as applied to multifunctional complex molecules and provided prospects for de novo drug design of potent MSAAs with simpler structures than complex natural products.[56] Accordingly, our common pharmacophore proposal spurred tremendous interest among MSAA researchers for a variety of implications in drug design.

However, when cryo-electron microscopy (cryo-EM; electron crystallography) provided the first "crystal structure" of paclitaxel-bound Zn^{2+}-stabilized α,β-tubulin dimer sheet model (3.7 Å resolution),[57] the research interest of ourselves and others in this field naturally moved to the determination of the bioactive structure of paclitaxel in the protein (see later in this review article). Moreover, the cryo-EM structure of epothilone A in the Zn^{2+}-stabilized tubulin dimer model (2.89 Å resolution) did not show meaningful overlap with the cryo-EM structure of paclitaxel.[58] Thus, the common pharmacophore concept appeared to have lost ground for several years until a very different tubulin-bound structure of epothilone A was elucidated by solution NMR spectroscopy with the real tubulin/microtubule in 2007.[59] The NMR structure of the tubulin–epothilone A complex was found to partially overlap with the structure of the paclitaxel–tubulin dimer sheet model stabilized by zinc ion, and SAR study results on epothilone analogues were nicely accommodated.[59] Thus, the common pharmacophore concept was fully revived from this point on. A 3D QSAR-based pseudoreceptor model for epothilone A (**3a**) and paclitaxel based on a common pharmacophore concept was proposed in 2003, which accommodated the SAR and mutagenesis results well.[60] Nevertheless, this pseudoreceptor model also had to wait until the appearance of the critical NMR study mentioned above in order to be validated. This model predicted the common pharmacophore for paclitaxel and epothilone B (**3b**) as illustrated in Figure 8, which has close

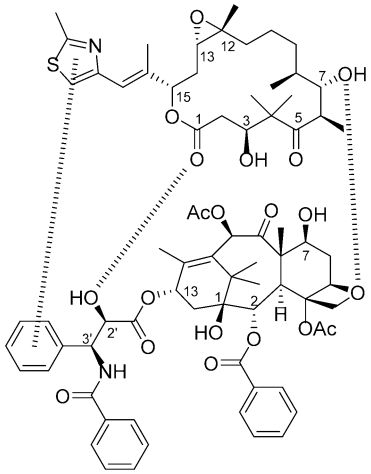

Figure 8. Common pharmacophore of paclitaxel and epothilone B (**3b**).

similarity to the one we proposed back in 1999 (see Figure 6b). Further validation of this common pharmacophore was performed by the synthesis of a number of epothilone analogues and their SAR analysis.[61]

(−)-Zampanolide (**7**) is another macrolide isolated from a marine sponge[62] and was only recently added to the list of MSAAs.[63] The X-ray crystal structure of the zampanolide–tubulin complex was determined at 1.8 Å resolution in 2013.[64] The zampanolide molecule was deeply buried in the taxane binding pocket formed by hydrophobic residues, and C-9 of zampanolide (**7**) was covalently bound to His^{229} of β-tubulin. Also, the side chains of zampanolide (**7**) and epothilone A (**3a**) showed an excellent overlap, indicating the existence of a common pharmacophore. Thus, our original common pharmacophore concept is still alive and thriving for a variety of MSAAs.

IDENTIFICATION OF TAXOL BINDING SITE IN TUBULIN AND ITS BIOACTIVE CONFORMATION

Photoaffinity Probes of Paclitaxel. Dr. Horwitz investigated the binding site of paclitaxel in tubulin/microtubules by photoaffinity labeling by using the radio-labeled photoreactive

DOI: 10.1021/acs.jnatprod.7b01012
J. Nat. Prod. 2018, 81, 703–721

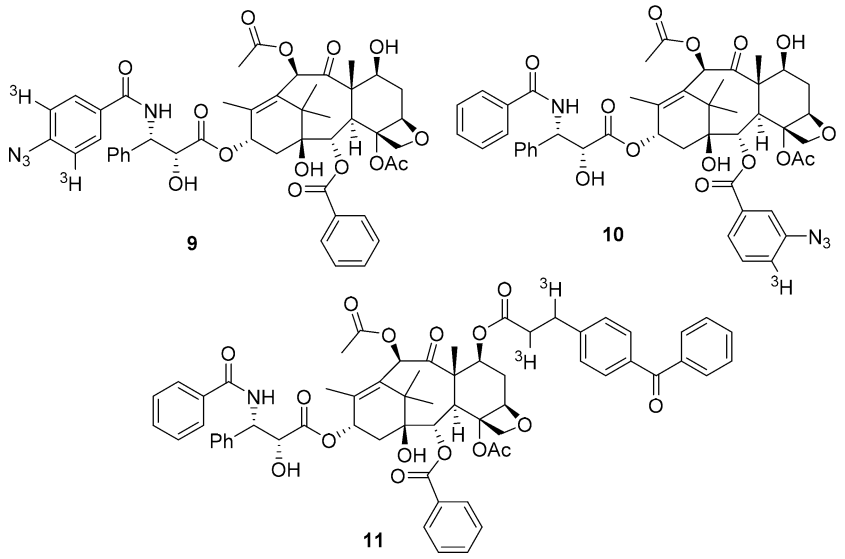

Figure 9. Photoaffinity probes and fluorine probes of paclitaxel.

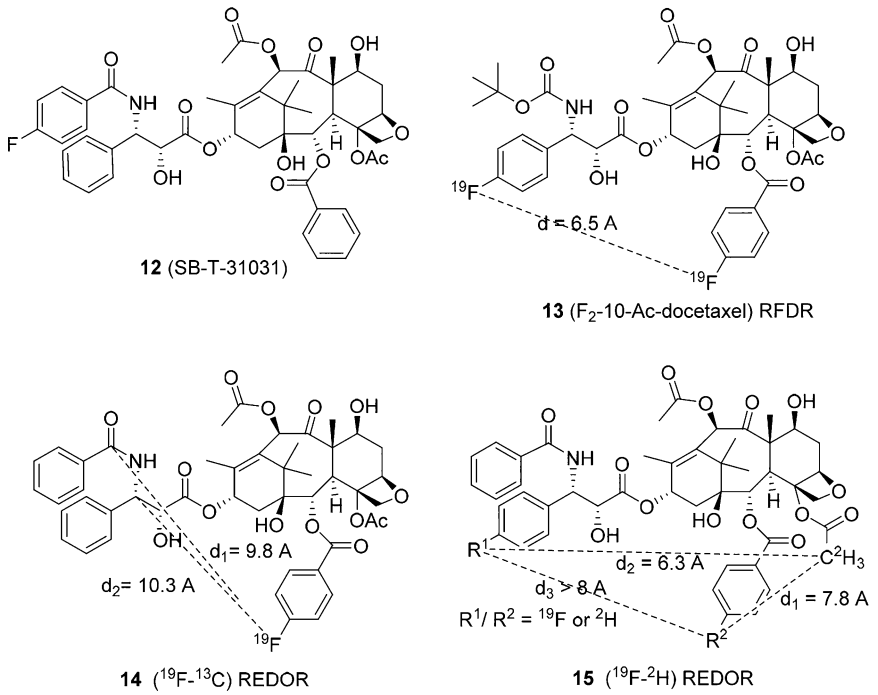

Figure 10. Fluorine probes of paclitaxel for solution and solid-state NMR studies.

paclitaxel analogues [^{3}H]3′-(*p*-azidobenzamido)paclitaxel (**9**)[65] and [^{3}H]2-(*m*-azidobenzoyl)paclitaxel (**10**)[66] (see Figure 9). Both probes photolabeled the N-terminal domain of *β*-tubulin specifically. Probe **9** led to the identification of the peptide fragment with the 1−31 amino acid residues,[65] while probe **10** verified the peptide fragment with the 217−231 amino acid residues.[66]

Although these two photoaffinity labeling results provided critical information that paclitaxel binds to the *β*-tubulin subunit near the interface with the *α*-tubulin subunit, it was still not possible to pinpoint the exact binding site as a result.

Accordingly, we collaborated with Dr. Horwitz to carry out a third photoaffinity labeling using [^{3}H]7-(benzoyldihydrocinnamoyl)paclitaxel (**11**). This experiment originally identified the peptide fragment with 277−293 amino acid residues of *β*-tubulin. Very fortunately, the subsequent sequence analysis led to the unambiguous determination of Arg282 as the single amino acid residue to which the benzophone radical was incorporated.[67] This was an exciting finding since it became possible for us to construct a highly plausible binding site for paclitaxel based on computer modeling. We found that our computationally identified paclitaxel binding site and the position of the baccatin skeleton in the real microtubules were in good agreement with those determined by the cryo-EM of the paclitaxel-bound Zn^{2+}-stabilized tubulin dimer model.[67] However, it was still not possible to determine the bioactive conformation of the *N*-benzoylphenylisoserine side chain at C-13 of paclitaxel.

Cryo-EM Structure of Paclitaxel Bound to Zn^{2+}-Stabilized Tubulin Dimer Model. The first cryo-EM

DOI: 10.1021/acs.jnatprod.7b01012
J. Nat. Prod. 2018, 81, 703−721

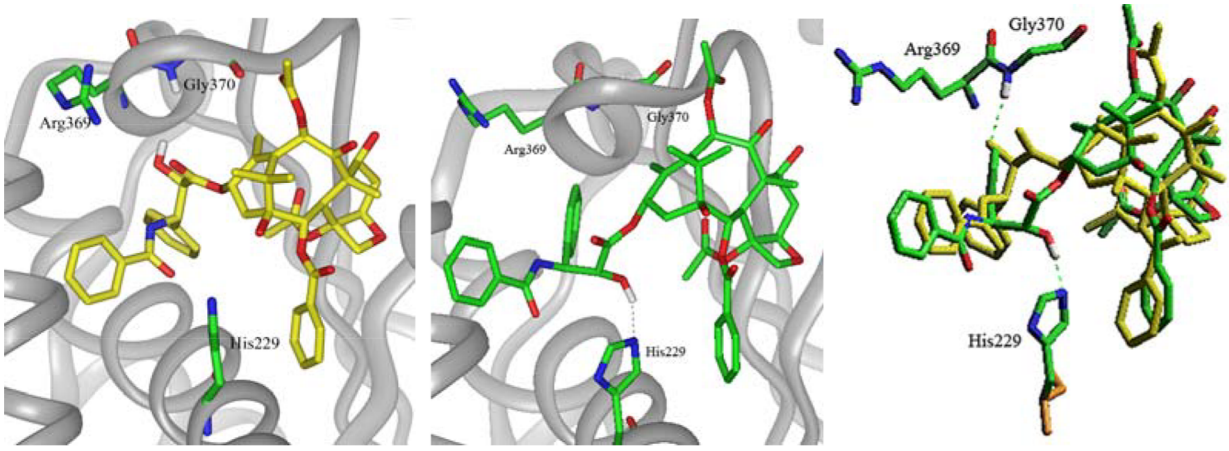

Figure 11. (a) "T-Taxol" in 1TUB. (b) "REDOR-Taxol" in 1JFF. (c) Overlay of "T-Taxol" and "REDOR-Taxol" in 1JFF. Adapted from ref 75 with permission.

(electron crystallography) structure of the paclitaxel–tubulin complex was reported in 1998, which used a Zn^{2+}-induced α,β-tubulin dimer sheet at 3.7 Å resolution (PDB: 1TUB). The electron density map clearly showed the baccatin skeleton and one of the side chains. For the determination of the position of baccatin, the first two photoaffinity labeling results made an important contribution. Based on the 1TUB structure and computational analysis, the "T-Taxol" structure was proposed in 2001 as the tubulin-bound bioactive from of paclitaxel (see Figure 11).[68] The 1TUB structure was further refined to 3.5 Å resolution (PDB: 1JFF) in 2001.[69] In this structure, the overall tubulin folding remains almost the same, while the geometry and side-chain positions are better defined than the 1TUB structure, revealing multiple amino acid residues in β-tubulin that were involved in paclitaxel binding.

Use of Fluorine Probes for the Structural Analysis of Paclitaxel in Solution and in Protein. The use of ^{19}F NMR methods for the conformational analysis of paclitaxel in solution, as well as in the solid state (protein), has produced critically important findings. For example, a fluorine probe, SB-T-31031 (**12**), was used for the analysis of dynamic conformational changes to successfully characterize three conformers in different solvent systems based on variable-temperature NMR techniques, exploiting the wide dispersion of ^{19}F chemical shifts, combined with the measurement of temperature dependence of vicinal proton coupling in the phenylisoserine side chain, as well as $^{19}F-^{1}H$ heteronuclear NOE measurements.[55] Another fluorine probe, F_2-10-Ac-docetaxel (**13**), was used for the determination of intramolecular $^{19}F-^{19}F$ distance based on homonuclear NOE when it was bound to tubulin in the solid state by applying solid-state magic angle spinning (SSMAS) ^{19}F NMR with the radio frequency driven dipolar recoupling (RFDR) pulse sequence. This pioneering SSMAS-RFDR work was performed in collaboration with Dr. Ann McDermott (Columbia University, New York), Dr. M. Lane Gilchrist (Columbia University/City University of New York, New York), and Dr. Horwitz.[70] The F–F distance for the two F atoms in the tubulin-bound **13** was determined to be 6.5 ± 0.5 Å, which suggested that this structure would have been formed via a small distortion of a solution conformation.[70]

For the SSMAS applications to the structural analysis of protein-bound small molecules, the rotational echo double resonance (REDOR) pulse sequence emerged as a powerful technique to accurately determine intramolecular atom–atom distances based on heteronuclear NOE. Thus, [^{13}C,^{15}N]-2-(4-fluorobenzoyl)paclitaxel (**14**)[71] and tetradeutero(fluoro)-paclitaxel (**15**)[72] were used to determine several intramolecular $^{19}F-^{13}C$ and $^{19}F-^{2}H$ distances in these fluoropaclitaxel molecules. The first $^{19}F-^{13}C$ REDOR distances were reported in 2000, and the second $^{19}F-^{2}H$ distances were determined in 2007. The distances thus determined were used for computational analyses to deduce the tubulin-bound paclitaxel structure. Thus, the "T-Taxol" structure satisfied those intermolecular atom–atom distances indicated by REDOR NMR.[71,72]

However, our Monte Carlo conformation search guided by the first REDOR-NMR data for fluoropaclitaxel **13** produced 16 possible conformations. Next, the structure with the least deviation from the two $^{19}F-^{13}C$ REDOR distances was selected as the best structure, which was named "REDOR-Taxol" in 2005 (see Figure 11).[73] The major difference between the "REDOR-Taxol" and "T-Taxol" structures is the H-bonding interaction of the OH-2′ group in the phenylisoserine side chain with β-tubulin. In the "T-Taxol" structure, the OH-2′ served as a H-bond acceptor to interact with the NH of Gly370 at the loop connecting strands B9 and B10, while in the "REDOR-Taxol" structure, the OH-2′ acts as a H-bond donor interacting with His 229.[73] The well-known SAR study indicates that OH-2′ should serve as a H-bonding donor.[74] This conclusion was, however, challenged by the report of an additional three $^{19}F-^{2}H$ REDOR distances determined by a second REDOR-NMR study in 2007,[72] which provided data that favored the T-Taxol conformation over the REDOR-Taxol conformation. A subsequent study using 1JFF in place of 1TUB for both "T-Taxol" and "REDOR-Taxol" for optimization confirmed that both structures satisfied REDOR distance constraints well.[75] When 1JFF was used, the proposed H-bonding of the C2-OH with Gly370 in "T-Taxol" was found to be unstable in molecular dynamics (MD) simulations, while that of "REDOR-Taxol" with His229 was very stable.[75]

Conformationally Constrained Paclitaxel Analogues Mimicking "T-Taxol" and "REDOR-Taxol". Rigidified macrocyclic paclitaxel analogues were designed and synthesized to mimic the "T-Taxol" and "REDOR-Taxol" structures. This is a logical approach to validate the relevance of these two proposed bioactive structures. Dr. Kingston's team synthesized several C-4–C-3′-linked macrocyclic paclitaxel analogues to support the "T-Taxol" structure, while our laboratory

DOI: 10.1021/acs.jnatprod.7b01012
J. Nat. Prod. 2018, 81, 703–721

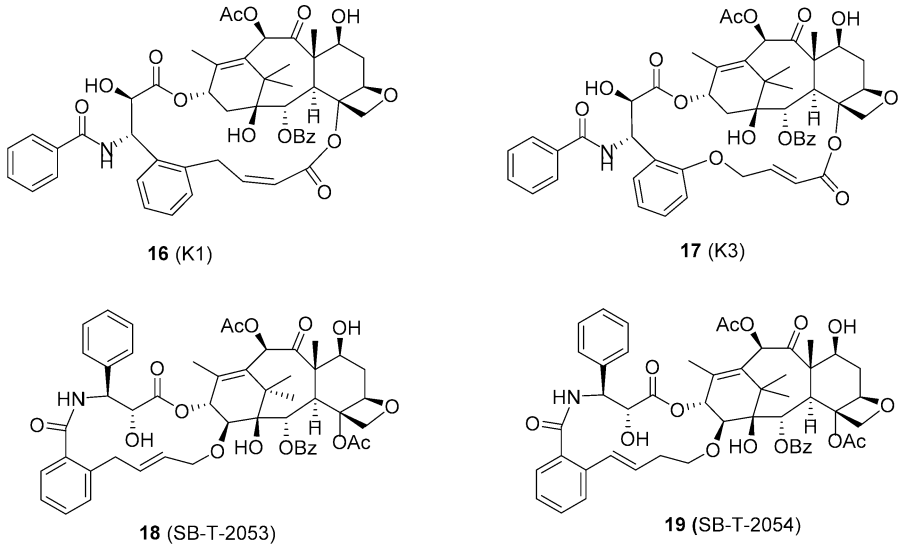

Figure 12. Macrocyclic paclitaxel analogues mimicking "T-Taxol" and "REDOR-Taxol".

constructed several C-14−C-3′NBz-linked macrocyclic paclitaxel analogues to support the "REDOR-Taxol" structure. Representative molecular structures of these novel macrocyclic paclitaxel mimics are shown in Figure 12.

Paclitaxel mimic K1 (**16**) exhibited substantially better activity than paclitaxel in a tubulin polymerization assay (2×) and in a cytotoxicity assay (20×) against the A2780 human ovarian cancer cell line.[76−78] The related mimic K3 (**17**) also showed the same activity as **16** in the tubulin polymerization assay, but an equal potency to paclitaxel in cytotoxicity assays against the PC3 human prostate and A2780 human ovarian cancer cell lines.[77] Mimic **17** was reported to take the "T-Taxol" structure as the predominant form (83%) in $CDCl_3$ based on the NMR analysis for flexibility in solution (NAMFIS[79]).[77]

Paclitaxel mimic SB-T-2054 (**19**) exhibited virtually the same activity as paclitaxel in the tubulin polymerization assay and in the cytotoxicity assay against the MCF7 (breast), NCI/ADR (ovarian), LCC6-WT (breast), LCC6-MDR (breast), and HT-29 (colon) human cancer cell lines.[80] The microtubules formed with **16** and paclitaxel were found to be very similar, while those formed with GTP are known to be longer and more uniform. Mimic SB-T-2053 (**18**), a double-bond regioisomer of **19**, showed slightly better activity than paclitaxel in the tubulin polymerization assay, but exhibited slightly weaker cytotoxicity than paclitaxel.[73] Both macrocyclic mimics take a virtually perfect "REDOR-Taxol" structure in computer modeling, and those structures are very stable in the MD simulations.[75,80]

Detailed computational analysis, including MD simulations for stability, of the "T-Taxol" mimic **16** and its saturated analogue has revealed that these mimics can readily take the "REDOR-Taxol" structure with the H-bonding of OH-2′ to His229 without any clash with the protein, and their "REDOR-Taxol" forms are very stable in the MD simulations.[75] Thus, it has been shown that **16**, **17**, and their congeners are not exclusive to the "T-Taxol" structure and mimic the "REDOR-Taxol" structure very well, too.

CHARACTERISTICS OF NEXT-GENERATION TAXOIDS IN CANCER CELL BIOLOGY

Tubulin Polymerization and Microtubule Dynamics. Next-generation taxoids were found to possess exceptional activity in promoting tubulin assembly, forming numerous very short microtubules,[22] in a manner similar to those formed by discodermolide, which has been recognized as the most potent naturally occurring microtubule-stabilizing agent.[44,81−83]

The activities of SB-T-1214 (**1**), SB-T-121303 (**20**), and SB-T-1213031 (**21**) on tubulin/microtubules were evaluated by tubulin polymerization assays using calf brain microtubule protein (MTP).[22] These three taxoids induced tubulin polymerization in the absence of GTP in a manner similar to paclitaxel (see Figures 13 and 14), and the microtubules formed

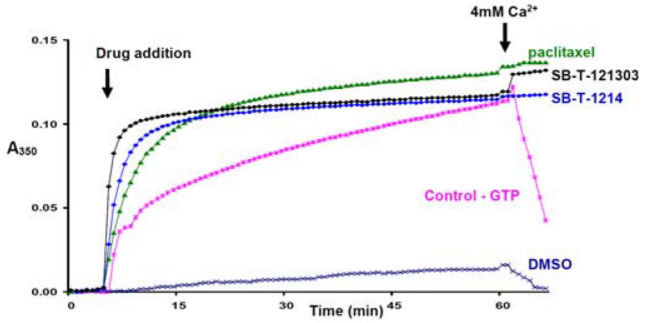

Figure 13. Tubulin polymerization with SB-T-1214 (**1**), SB-T-121303 (**20**), and paclitaxel: microtubule protein 1 mg/mL, 37 °C, GTP 1 mM, drug 10 μM. Adapted with permission from ref 22.

with these new-generation taxoids were stable against Ca^{2+}-induced depolymerization.[22] As Figure 13 shows, taxoids **1** and **20** promote the rapid polymerization of tubulin at a faster rate than paclitaxel. The turbidity of the tubulin solution treated by **1** or **20** reaches a plateau quickly and does not change with time. This observation may imply that there is a difference in structure between microtubules formed with the new-generation taxoids and those with paclitaxel. The third-generation taxoid **20** causes spontaneous tubulin polymerization, reaching >90% of a plateau within 5 min from onset, while it takes about 12 min for **1** to reach the same point.[22]

In a similar manner, the activity of **21** was compared with that of paclitaxel in a tubulin polymerization assay[22] using a protocol for tubulin preparation slightly different from that used for the experiments presented in Figure 13. As Figure 14

DOI: 10.1021/acs.jnatprod.7b01012
J. Nat. Prod. 2018, 81, 703−721

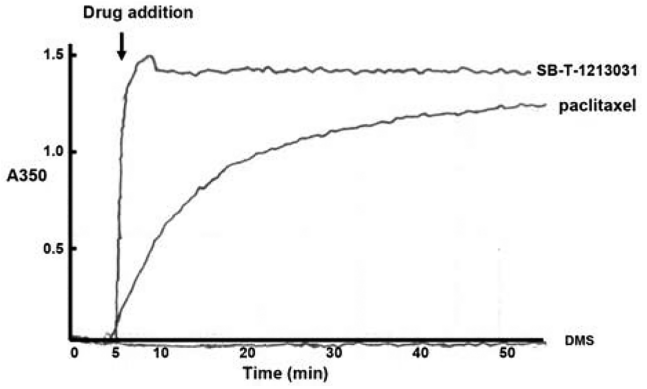

Figure 14. Tubulin polymerization with SB-T-1213031 (**21**): microtubule protein 1 mg/mL, 37 °C, GTP 1 mM, drug 10 μM. Adapted with permission from ref 22.

shows, this assay reveals a remarkable difference in the rate of tubulin polymerization between the third-generation taxoid **21** and paclitaxel. Taxoid **21** causes almost instantaneous polymerization of tubulin, completing the polymerization within 2 min, while paclitaxel promotes the polymerization much more slowly.[22]

Essentially the same results, i.e., rapid tubulin polymerization and stabilization of microtubules formed, were obtained for SB-T-1213 (**22**) and ortataxel,[84] as well as the difluorovinyltaxoids SB-T-12851 (**23**), SB-T-12852 (**24**), SB-T-12853 (**25**), and SB-T-12854 (**26**) (see Figure 15 for structures).[39]

The microtubules formed with the next-generation taxoids **1**, **20**, and **21** were analyzed further by electron microscopy for their morphology and structure in comparison with those formed by using GTP and paclitaxel.[22] As Figure 16A and B show, GTP and paclitaxel form long and straight microtubules. The microtubules formed with **1** (Figure 16C) are shorter than those with GTP or paclitaxel. In contrast, the morphology of the microtubules formed by the action of **20** and **21** is unique in that those microtubules are very short and numerous (Figure 16D and E). The microtubules with **20** appear to have more curvature than those with **21**. It is worth mentioning that discodermolide forms microtubules with characteristics similar to those formed with **20** and **21**, i.e., short and numerous (Figure 16F).[44,81−83] It is strongly suggested that the formation of short and numerous microtubules is related to the instantaneous rapid polymerization of tubulin observed with these third-generation taxoids as well as discodermolide.[22]

The microtubules formed by treatment of tubulin with three difluorovinyltaxoids, **23**, **24**, and **26**, were also analyzed by electron microscopy.[39] There was morphological similarity between those microtubules generated by the action of difluorovinyltaxoids and those by **21** and **1**, but the formation of thinner, shorter, and straight microtubules appears to be unique to difluorovinyltaxoids.[39]

Taxoid **22** induces the formation of unusual microtubules with attached extra protofilaments or open sheets, and ortataxel induces large protofilamentous sheets.[84] As Figure 17 shows, ortataxel (A and B) induced the formation of large bundles of fibers (asterisk), large sheets (arrows), and a few microtubules. Taxoid **22** (C and D) induced the formation of microtubules (M) and a few sheets (arrows), partial microtubules, loops and coils (C), and long regions of a small number of protofilaments associated linearly with microtubules. Paclitaxel (1 μM) (E and F) induced the formation of many microtubules (M) and few sheets or loops. The marked tendency of ortataxel and **22** to induce the polymerization of tubulin into sheets and other aberrant microtubule-like forms suggests that these next-generation taxoids induce conformational changes in tubulin/microtubules that differ significantly from the conformational changes induced by paclitaxel. Thus, the differences in the interactions of these taxoids with tubulin/microtubules are likely to play a role in their enhanced cytotoxicity and tumor efficacy as compared with paclitaxel.

Unique Thermodynamic Properties of Next-Generation Taxoids for Tubulin-Binding. The critical concentration of tubulin required for assembly induction in the presence of **1**, **20**, and **26** was determined and compared with those for paclitaxel using centrifugation and quantification of the microtubules formed (Table 1).[28] Apparently, these three next-generation taxoids induced tubulin assembly with much higher potency than paclitaxel and docetaxel. Thus, it is indicative that not only the rate of assembly was greater but also a larger number of microtubules was formed. It should be noted that fluorotaxoid **26** exhibited the strongest assembly induction power among the taxanes examined, with a critical concentration of 0.3 μM.

In order to correlate the observed cytotoxic effect of paclitaxel and these next-generation taxoids with their affinity to microtubules, the binding constants of these compounds were determined using a fluorescent ligand displacement method.[28] As Table 2 shows, the binding of **26** is ca. 10 times stronger than paclitaxel and slightly better than **1**, while a third-generation taxoid, **20**, binds to microtubules 270−330 times stronger than paclitaxel.[28]

Next, the thermodynamic parameters of the interaction, i.e., free energy of the binding (ΔG) and the enthalpy (ΔH) and entropy (ΔS) contributions to ΔG, were calculated based on the binding constants.[28] As Table 3 indicates, the binding of these three next-generation taxoids is much less exothermic with a large decrease in the enthalpy of binding, but this decrease in the enthalpy of binding was compensated for by a substantial increase in the entropy of binding, which suggests significant differences in the binding mechanism.

NEWER INSIGHTS INTO THE MECHANISM OF ACTION

Significant Activity of Next-Generation Taxoids against Cancer Stem Cells and the Origin of Their High Potency. In the past decade, the ineffectiveness of conventional chemotherapeutic drugs has been attributed to the existence of relatively rare, highly drug-resistant, quiescent or slowly proliferating tumor-initiating cells, termed "cancer stem cells".[85,86] Through successful isolation and characterization of CSCs from all major types of human tumors, it has become evident that CSCs are exclusively endowed with tumor-initiating capacity for the majority of, if not all, cancer types. More importantly, there is every indication that CSCs are responsible for tumor maintenance, resistance to treatment, metastasis, and recurrence.[85] CSCs induce a variety of proliferating, but progressively differentiating tumor cells, contributing to the cellular heterogeneity of human cancers. Therefore, it appears that CSCs represent the most crucial target in the development of next-generation anticancer drugs.[87,88]

As described above, next-generation taxoid **1** demonstrated remarkable efficacy in drug-resistant cancers both in vitro and in vivo.[22] Taxoid **1** was also found to exhibit excellent activity

DOI: 10.1021/acs.jnatprod.7b01012
J. Nat. Prod. 2018, 81, 703−721

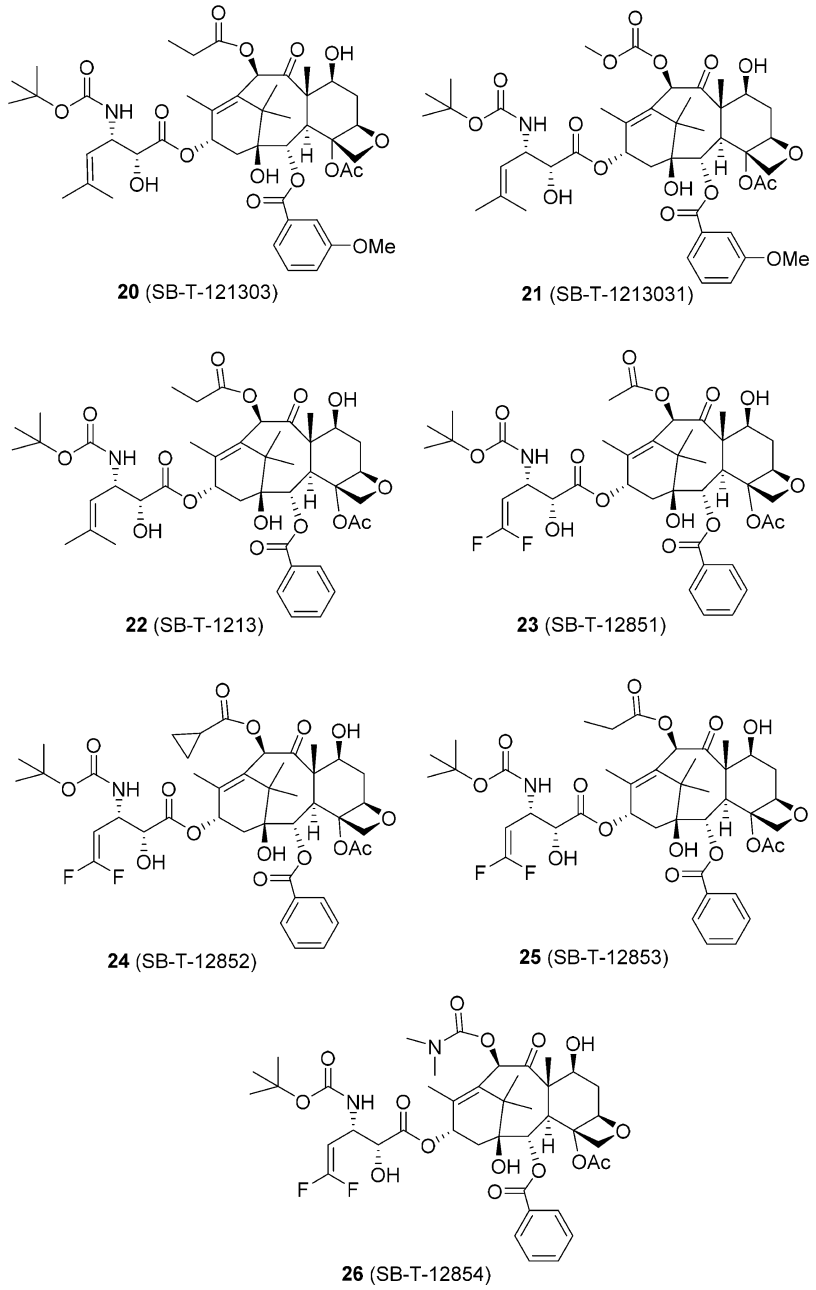

Figure 15. Selected structures of next-generation taxoids used in the tubulin polymerization assay.

against spheroids derived from highly drug-resistant CSCs.[87] A comparison of potencies between conventional anticancer drugs and new-generation taxoids is summarized in Table 4.[89] As Table 4 shows, it is impressive that these next-generation taxoids exhibited 41−33 000 times higher potency than conventional anticancer drugs against the CSC-enriched HCT-116 cell line. As CSCs are believed to be responsible for tumor metastasis and reoccurrence,[90] this finding is quite significant.

It has been indicated that next-generation taxoids, exhibiting high potencies against CSCs, suppress the expression of "stemness genes", promoting differentiation of the treated CSCs (Figure 18),[87] which may provide a new mechanism of action for taxoid anticancer agents for which the major MOA is the blocking of cell mitosis at the G2/M stage, leading to the activation of caspases and then apoptosis.[28,40,91−93]

Furthermore, we isolated $CD133^{high}/CD44^{high}$-expressing prostate CSCs from patient-derived PPT2 and metastatic PC3MM2 cells.[88] The cancer stem cells upregulate expression of stem-cell-related genes and are likely to form 3D colonospheres. Treatment of these CSCs with **1** for 48 h induced ca. 60% cell death in the tested prostate CSCs.[88] It should be noted that the CSCs that survived taxoid **1** treatment exhibited abnormal morphology and were unable to form secondary floating spheroids. Taxoid **1** treatment remarkably downregulated the expression of stem-cell-relevant transcription factors in prostate CSCs and moderately downregulated the expression of pluripotency-related transcription factors c-Myc and Sox2.[88] Taxoid **1** treatment induced expression of pro-apoptotic/tumor-suppressor proteins p21 and p53 through "gene wake-up".[88] In vivo treatment of PPT2 and PC3MM3 tumor-bearing NOD/SCID mice with **1** weekly

DOI: 10.1021/acs.jnatprod.7b01012
J. Nat. Prod. 2018, 81, 703−721

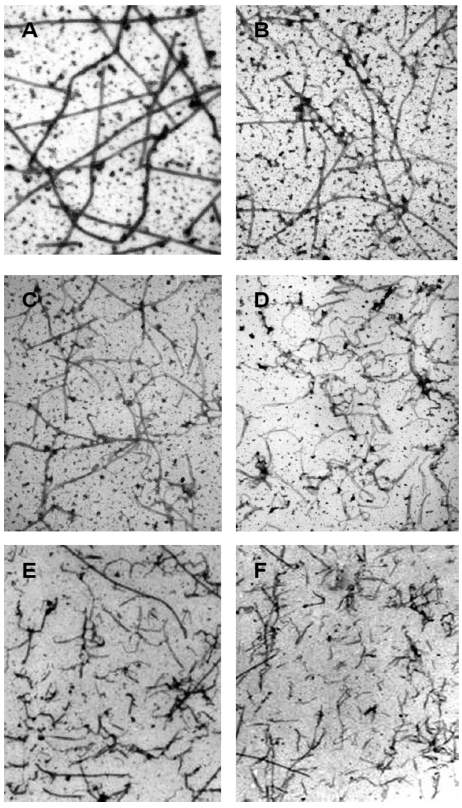

Figure 16. Electromicrographs of microtubules (20 000×): (A) GTP; (B) paclitaxel; (C) SB-T-1214 (**1**); (D) SB-T-121303 (**20**); (E) SB-T-1213031 (**21**); (F) discodermolide. Copied from ref 22.

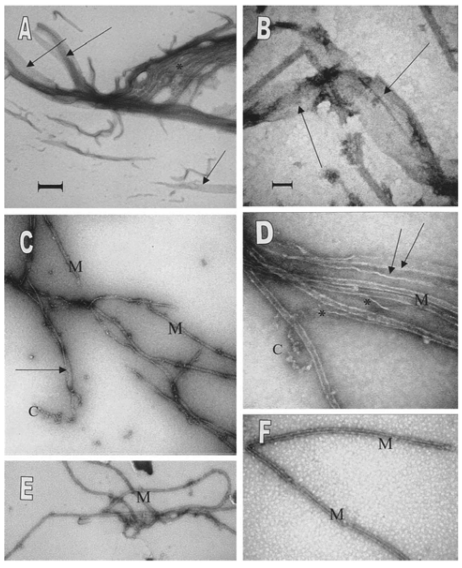

Figure 17. Tubulin polymers induced by 1 μM ortataxel or 1 μM SB-T-1213 (**22**), as compared to paclitaxel. Electron micrographs: left column, low magnification; right column, high magnification. The scale bar in A represents 500 nm; that in B represents 100 nm. A, C, and E are at the same magnification, as are B, D, and F. Adapted from ref 84 with permission.

(i.v.) for 4 weeks suppressed tumor growth and even led to tumor eradication in some of the mice.[88]

Suppression of Hedgehog Signaling Pathway. The Hedgehog (HH) signaling pathway is one of the major pathways in pancreatic ductal adenocarcinoma (PDAC).[94] The prognostic importance of the HH pathway was investigated in pancreatic cancer patients who underwent a radical resection.[95] Tumors and adjacent non-neoplastic pancreatic tissues were obtained from 45 patients with histologically verified pancreatic cancer. The effect of next-generation taxoid **2** on the expression of the HH pathway was evaluated in vivo using a mouse xenograft model prepared using pancreatic cancer cell line Paca-44.[95] The transcription profile of 34 HH pathway genes in patients and xenografts was assessed using quantitative PCR. The HH pathway was strongly overexpressed in pancreatic tumors, and upregulation of SHH, IHH, HHAT, and PTCH1 was associated with a trend toward decreased patient survival.[95] No association of Hedgehog pathway expression with KRAS mutation status was found in tumors. It was found that a sonic HH ligand was overexpressed, and all other downstream genes were downregulated by taxoid **2** treatment in vivo.[95] Effective suppression of the HH pathway expression in vivo by a next-generation taxoid may provide a bright prospect in the

Table 1. Critical Concentration (μM) of Tubulin Required for Microtubule Assembly

compound	critical tubulin concentration
DMSO (vehicle)	>200
paclitaxel	4.2 ± 0.2
1 (SB-T-1214)	0.9 ± 0.2
20 (SB-T-121303)	0.6 ± 0.1
26 (SB-T-12854)	0.3 ± 0.1

Table 2. Binding Constants of Taxanes with Microtubules ($\times 10^7$ M^{-1})

compound	26 °C	35 °C
paclitaxel	2.64 ± 0.17	1.43 ± 0.17
1 (SB-T-1214)	12 ± 2	8 ± 2
20 (SB-T-121303)	731 ± 82	478 ± 47
26 (SB-T-12854)	15 ± 3	10 ± 3

Table 3. Thermodynamic Parameters of Binding of Taxanes to Microtubules

compound	Δ*G* 35 °C (kJ/mol)	Δ*H* (kJ/mol)	Δ*S* (kJ/mol)
paclitaxel	−42.1 ± 0.3	−51 ± 4	−29 ± 13
1 (SB-T-1214)	−46.6 ± 0.6	−32 ± 2	47 ± 6
20 (SB-T-121303)	−57.0 ± 0.2	−31 ± 2	87 ± 7
26 (SB-T-12854)	−47.1 ± 0.7	−28 ± 3	64 ± 10

Table 4. Cytotoxicity (IC_{50} nM) of Standard Anticancer Drugs and New-Generation Taxoids against the CSC-Enriched (CD133++) HCT-116 Human Colon Cancer Cell Line

anticancer agent	IC_{50} (nM)
cisplatin	4,540 ± 276
doxorubicin	78.0 ± 28.2
methotrexate	32.7 ± 11.2
paclitaxel	33.8 ± 3.33
topotecan	451 ± 12
1 (SB-T-1214)	0.28 ± 0.10
2 (SB-T-1216)	0.83 ± 0.05
26 (SB-T-12854)	0.14 ± 0.05
27 (SB-T-121602)[a]	0.24 ± 0.13

[a]See Figure 19 for the structure of SB-T-121602 (**27**).

DOI: 10.1021/acs.jnatprod.7b01012
J. Nat. Prod. 2018, 81, 703−721

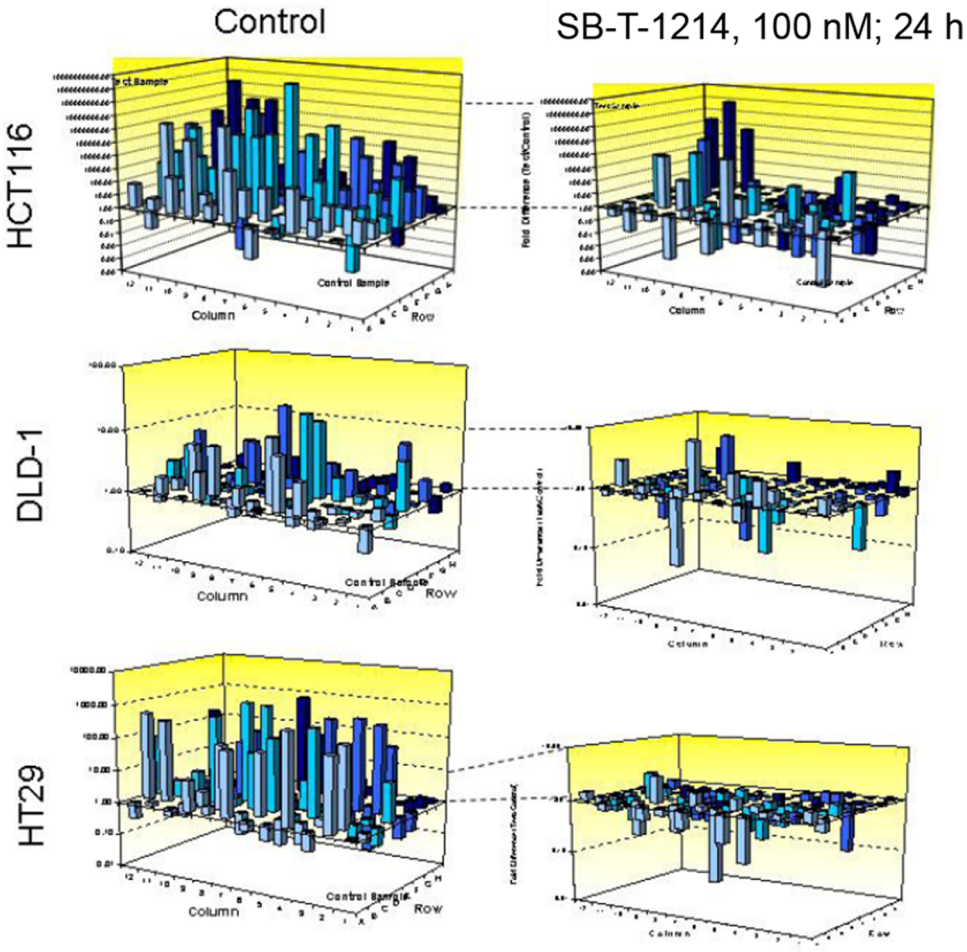

Figure 18. Drug-induced alteration in the stem-cell-related gene expression profiles (PCR array assay). A majority of the stemness genes were upregulated in floating spheroids grown from $CD133^{high}/CD44^{high}$ cells derived from HCT116, HT29, and DLD-1 cell lines in comparison with their corresponding bulk counterparts (left panel). Treatment of colonospheres with 100 nM SB-T-1214 (**1**) induced significant downregulation of a majority of the stemness genes. Adapted from ref 87 with permission.

efficacious treatment of this aggressive tumor by exploiting this newly revealed MOA involving the HH pathway.

Suppression of the PI3K/Akt Pathway. Several next-generation taxoids were screened against an extremely paclitaxel-resistant MCF-7/PTX human breast cancer cell line, developed by Dr. Yalin Dong's laboratory (Xi'an Jiaotong University, China) as shown in Table 5. Among these second- and third-generation taxoids, two third-generation taxoids, **20** and SB-T-121205 (**28**), exhibited the best cytotoxicity, and **28** was selected for detailed mechanistic studies. The structures of SB-T-101141 (**31**) and three CF_3O-containing taxoids (**28**–**30**) are shown in Figure 19.

Table 5. Effect of Paclitaxel and Next-Generation Taxoids on Cell Viability in MCF-7/PTX Cells

taxane	IC_{50} (nM)
paclitaxel	2290.87 ± 125.18
1 (SB-T-1214)	80.50 ± 7.62
20 (SB-T-121303)	21.67 ± 2.25
28 (SB-T-121205)	19.01 ± 2.03
29 (SB-T-121405)	34.90 ± 2. 97
30 (SB-T-121605)	31.43 ± 2.84
31 (SB-T-101141)	66.66 ± 5.59

SB-T-121205 (**28**) exhibits much higher potency against drug-sensitive and drug-resistant human breast cancer cell lines (MCF-7/S, MCF-7/PTX, and MDA-MB-453) than paclitaxel, while this taxoid was less toxic to nontumorigenic human bronchial epithelial cells (BEAS-2B) as compared to paclitaxel.[96] Flow cytometry and Western blot analyses revealed that **28** induced cell cycle arrest at the G2/M phase and apoptosis in MCF-7/PTX cells by the accelerating mitochondrial apoptotic pathway, resulting in the reduction of the Bcl-2/Bax ratio, as well as elevation of caspase-3, caspase-9, and poly(ADP-ribose)polymerase (PARP) levels. Taxoid **28** inhibited cell migration and invasion in the wound-healing-scratch and Transwell-invasion assays. Furthermore, the mammosphere-forming ability of MCF-7/PTX cells, as well as their migration and invasion abilities, was suppressed by SB-T-121205 treatment. The Western blot assay indicated that **28** treatment increased the expression of the epithelial marker E-cadherin and decreased that of mesenchymal markers N-cadherin and vimentin, which indicated that **28** inhibited cell migration in the Snail pathway. Treatment with **28** downregulated the expression of transgelin 2, p-Akt, and p-GSK-3β and upregulated the expression of tumor-suppressor PTEN. The results indicate that SB-T-121205 inhibits migration/invasion and exhibits cytotoxicity by suppressing the PI3K/Akt pathway in MCF-7/PTX cells,[96] which indicated that selected next-

DOI: 10.1021/acs.jnatprod.7b01012
J. Nat. Prod. 2018, 81, 703−721

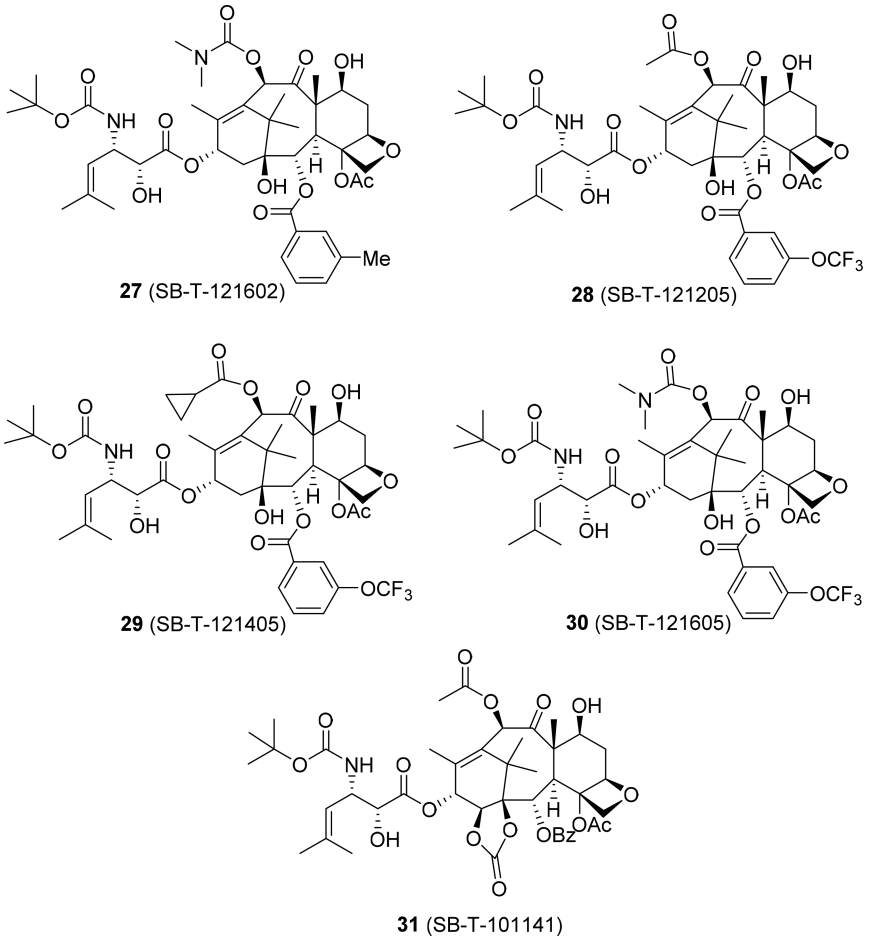

Figure 19. Selected structures of next-generation taxoids used in the cytotoxicity assays.

generation taxoids would be able to prevent metastasis and suppress epithelial−mesenchymal transition besides killing cancer cells via enhancement of apoptosis. These are MOAs that have not been known for classical taxane anticancer agents such as paclitaxel and docetaxel and warrant further investigations to advance cancer chemotherapy.

TUMOR-TARGETED DRUG DELIVERY OF NEXT-GENERATION TAXOID ANTICANCER AGENTS

Traditional chemotherapy depends on the premise that rapidly proliferating tumor cells are more likely to be destroyed by cytotoxic agents than normal cells. In reality, however, these cytotoxic agents have little or no specificity, which leads to systemic toxicity, causing undesirable side effects. Accordingly, the development of tumor-specific drug delivery systems for anticancer agents, differentiating the normal tissues from cancer cells or tissues, is an urgent need to improve the efficacy of cancer chemotherapy. Various drug delivery systems have been studied over the past few decades to address this problem.[97] In general, there are two types of tumor targeting strategies, i.e., passive targeting and active targeting. Both strategies can enhance selective accumulation and residence time of anticancer drugs in tumor.[98]

Passive and Active Tumor-Targeting. Passive tumor-targeting is based on biophysiological properties of tumor tissues, e.g., numerous leaky blood vessels and the lack of a lymphatic drainage system in the tumor.[99] This strategy takes advantage of the EPR effect[100] of macromolecule- and nanoparticle-based vehicles (10−500 nm in size), which is specific to tumor tissues, resulting in selective accumulation of cytotoxic agents in a tumor.[99] Rapidly growing cancer cells overexpress tumor-specific receptors to enhance the uptake of nutrients and vitamins. These receptors can be used for active tumor-targeting, enabling cancer cell-specific delivery of cytotoxic agents through receptor-mediated endocytosis (RME). Furthermore, the characteristic physiology of tumor and cancer cells can be exploited to selectively accumulate and release a cytotoxic agent inside these cells. For example, monoclonal antibodies, peptides, aptamers, polyunsaturated fatty acids, folic acid, biotin, and hyaluronic acid have been employed as tumor-specific targeting modules to construct tumor-targeting drug conjugates.[97,98,101−104] Next-generation taxoid anticancer agents certainly serve as potent payloads for the tumor-targeting drug conjugates.[105]

As a general structure, tumor-targeting drug conjugates (TTDCs) consist of a tumor-targeting module (TTM) conjugated to a cytotoxic payload through a suitable "smart" linker. These drug conjugates should be stable in blood circulation to minimize systemic toxicity and should be effectively internalized inside the target tumor cells. Upon internalization, the drug conjugate should efficiently release the cytotoxic agent without loss of potency. Thus, the "smart" linkers should possess proper characteristics to provide suitable stability and reactivity. Owing to the critical importance of linker dynamics for the efficacy of tumor-targeted drug delivery,

DOI: 10.1021/acs.jnatprod.7b01012
J. Nat. Prod. 2018, 81, 703−721

various smart linker systems have been developed in the last two decades, in particular for antibody−drug conjugates (ADCs)[97,102,106−110] and small-molecule drug conjugates (SMDCs).[97,111−115] In this regard, we have developed novel self-immolative disulfide linkers that can release unmodified cytotoxic drugs (Figure 20).[105,114−119]

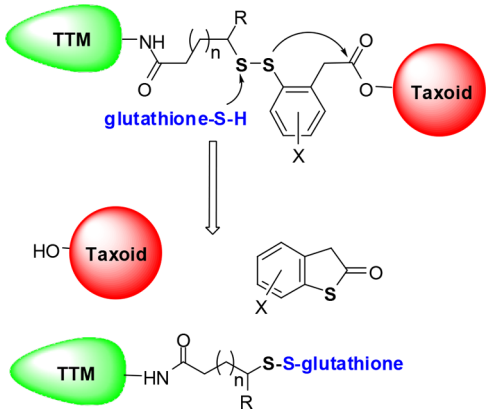

Figure 20. Structure and drug release mechanism of disulfide linker. Adapted from ref 117.

Vitamin B Receptors as Targets. Folic acid (vitamin B_9), a tetrahydrofolate precursor, is required in DNA synthesis and reparation.[120] The corresponding folate receptor (FR) is overexpressed in a good number of tumors and absent in most normal tissue.[103] Biotin (vitamin B_7) is a water-soluble vitamin involved in the regulation of epigenetics,[121] the synthesis and/or metabolism of fatty acids,[122] and energy production. The biotin receptors (BRs) are overexpressed in a wide variety of cancer cells, and the expression levels are even higher than folate and vitamin B_{12} receptors in many cancer cells.[123,124] Thus, BR is an excellent target for tumor-targeted drug delivery.[114]

Figure 21 exemplifies a series of taxoid-based TTDCs using self-immolative disulfide linkers, which have been successfully developed in our laboratory.[114,115,117,118] These TTDCs, biotin−linker−taxoid (BLT) and folate−linker−taxoid (FLT), targeting vitamin B receptors, are efficiently internalized via RME, which transfers the drug conjugates through endosomal and lysosomal compartments. It has been shown that the concentration of endogenous thiols, represented by glutathione (GSH), in these compartments is >1000 times higher (2−8 mM) than that in the bloodstream (1−2 μM).[125,126] GSH and other thiols trigger the drug release cascade of the self-immolative linker system via the cleavage of disulfide linkage and thiolactonization (Figure 20).[117,127] The internalization of TTDCs via RME and designed drug release inside cancer cells were clearly visualized and validated by confocal fluorescence microscopy (CFM) and flow cytometry analyses, using fluorescence-labeled TTDCs.[114,115,117,118] These TTDCs demonstrated 2−3 orders of magnitude enhanced selectivity and potency against a variety of cancer cells overexpressing biotin or folate receptors (BR+, FR+), as compared to normal human fibroblast cells with only natural level of vitamin B receptors (BR−, FR−).[114,128]

The in vivo study of a BLT conjugate (with taxoid **1**) against MX-1 triple-negative human breast tumor xenografts in SCID mice exhibited remarkable efficacy via i.v. administration weekly for 4 weeks, wherein all tumors were eradicated without recognizable body weight loss in all mice examined, while a conventional treatment with the same taxoid itself was found to need much higher doses to show tumor regression with considerable systemic toxicity.[129]

This TTDC platform was readily applied to a novel drug conjugate bearing two different anticancer agents, i.e., taxoid **1**, targeting microtubules, and camptothecin (CPT), targeting topoisomerase I, in one molecule ("dual-warhead" conjugate, Figure 21). This type of dual-warhead conjugate provides a new approach to combination therapy.[115]

A theranostic biotin−taxoid conjugate (Figure 21), incorporating a fluorine-labeled prostheric for potential ^{18}F-PET imaging, was constructed, which exhibited excellent cancer cell selectivity (>100) to BR+ cancer cells as compared to BR− human normal cells.[119]

Antibody−Drug Conjugates. Cancer cells overexpress certain antigens on the cell surface, and these tumor-specific antigens can be used as biomarkers to differentiate tumor tissues from normal tissues.[97,109,130] Certain monoclonal antibodies (mAb) have high binding specificity to tumor-specific antigens and can be used as drug delivery vehicles to carry a payload of cytotoxic agents specifically to the tumor site. The mAb−drug conjugate is internalized upon binding to the tumor antigen via RME, and the payload is released inside the cancer cell. We successfully conjugated a highly cytotoxic C-10-methyldisulfanylpropanoyltaxoid to immunoglobin G class mAbs, recognizing the epidermal growth factor receptor, through a disulfide-containing linker (Figure 21).[108] These conjugates showed excellent selectivity in vitro and remarkable antitumor activity in vivo against A431 human squamous tumor xenografts in SCID mice, resulting in eradication of the tumor without appreciable systemic toxicity.[108] This pioneering work on taxoid-based ADCs was published in 2002,[108] well preceding the current explosive development of ADCs in clinical trials for cancer chemotherapy, stimulated by recent FDA approvals of Adcetris (brentuximab vedotin)[131] and Kadcyla (ado-trastuzumab emtansine).[132]

However, the modification at the C-10 position of the taxoid resulted in 8−10 times loss of potency relative to the parent taxoid.[108] Accordingly, a mechanism-based second-generation linker system was designed and developed to allow the release of the unmodified taxoid with uncompromised potency, as described above (Figure 20).

Nanoscale Vehicles for Taxoid Delivery. Besides mAbs, which are nanoscale biomaterials, we have investigated and developed novel tumor-targeting drug conjugates and nanoparticles using nanoscale vehicles. Figures 22 and 23 exemplify nanoscale drug delivery systems with active and passive tumor-targeting, which have been developed in our laboratory. We successfully constructed a novel TTDC with single-wall carbon nanotubes (SWNTs), bearing multiple biotins and taxoids, wherein 178 biotin molecules and 71 taxoids (taxoid = SB-T-1214-fluorescein) are attached to a single SWNT of 250 nm in length and 1 nm in diameter (average) (Figure 22).[118] This huge "Trojan horse" TTDC was shown to be completely internalized by RME based on CFM analysis, as well as exhibited excellent cytotoxicity and cancer cell selectivity (>150) to BR+ cancer cells as compared to normal human cells (BR−), which clearly indicated the benefit by mass delivery of cytotoxic payload to cancer cells via RME.[118]

We have also constructed a unique asymmetric bowtie dendrimer (ABTD)-based TTDC, bearing 16 biotins in the G3 half-dendron moiety and four taxoids connected to self-

DOI: 10.1021/acs.jnatprod.7b01012
J. Nat. Prod. 2018, 81, 703−721

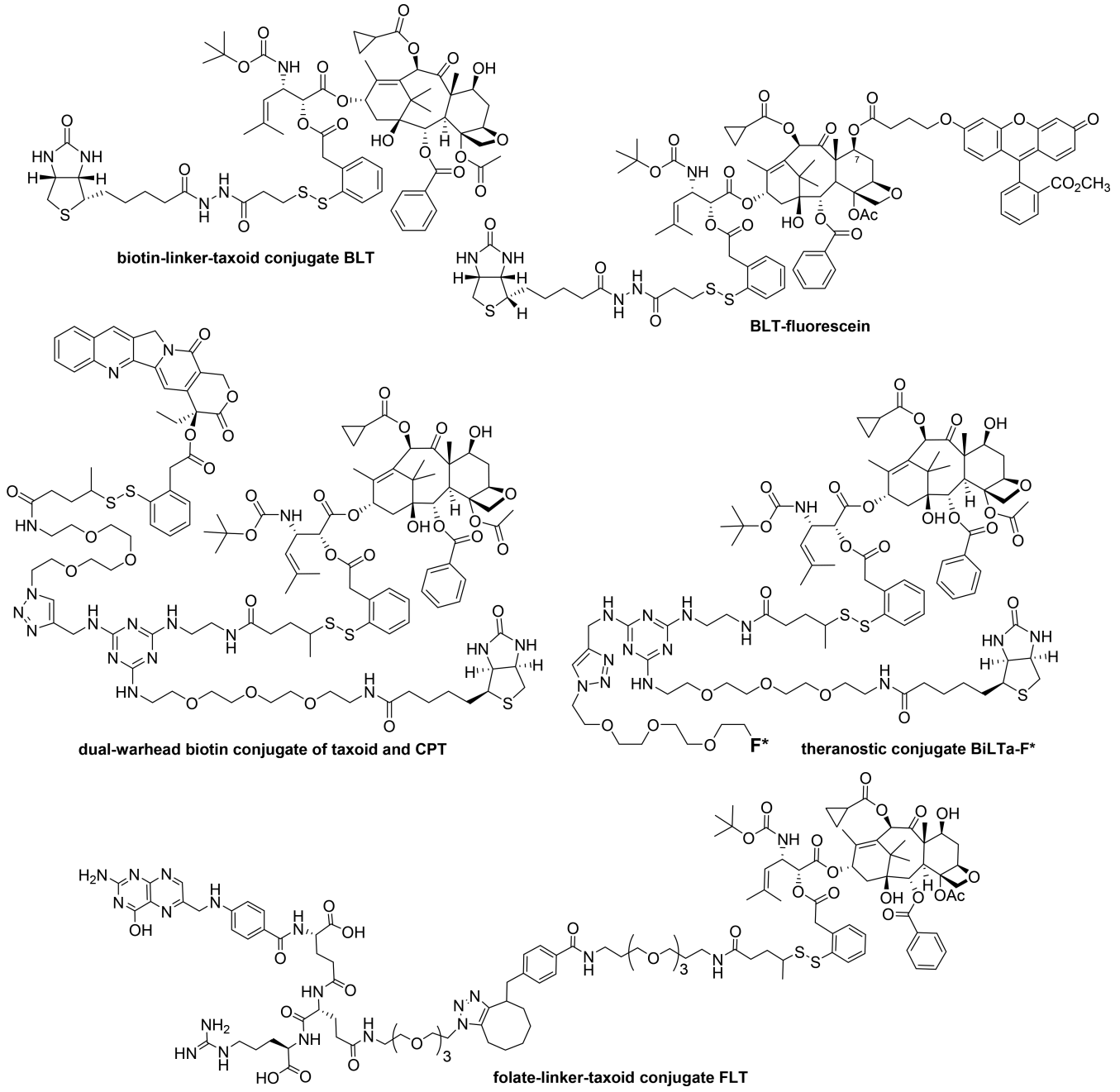

Figure 21. Taxoid-based SMDCs targeting vitamin B receptors.

immolative linkers in the G1 half-dendron moiety (Figure 22).[133] This asymmetric dendrimer was designed and synthesized from poly(amido amine) dendrimers with cystamine cores. This ABTD-TTDC exhibited remarkable cancer cell selectivity (1000−5000) to ID-8 ovarian and MX-1 breast cancer cell lines (BR+) as compared to WI38 human lung fibroblast cells (BR−).[133]

Poly(2-oxazoline)s (POx) micelle drug delivery systems were developed based on triblock copolymers of poly(2-methyl-2-oxazoline) and poly(2-butyl-2-oxazoline). The POx micelles exhibited high efficiency in solubilization of paclitaxel and next-generation taxoids. The small and highly loaded POx/SB-T-1214 micelles (<100 nm in diameter) exhibited 1−2 orders of magnitude higher activity than Pox/paclitaxel in drug-resistant LCC6/MDR human breast cancer cell line in vitro, as well as impressive in vivo efficacy in suppressing the growth of LCC6/MDR and T11 orthotropic tumors in mice models.[134]

Nanoemulsions (NEs) are emerging as an attractive drug delivery system to enhance the efficacy of drugs and to minimize exposure of therapeutic cargo to normal tissues, potentially reducing side effects. To improve therapeutic outcome with reduced toxicity, we developed a safe and effective, omega-3 rich polyunsaturated fatty acid (PUFA) containing an oil-in-water nanoemulsion loaded with a PUFA−taxoid conjugate, DHA-SB-T-1214, which has exhibited remarkable efficacy in vivo against various tumor xenografts in mice models, including highly drug-resistant DLD-1 (colon), PANC-1 (pancreatic), and CFPAC-1 (pancreatic) cancer cell lines,[135,136] but had some stability issues due to oxidation. The nanoemulsion of DHA-SB-T-1214 (NE-DHA-SB-T-1214)

DOI: 10.1021/acs.jnatprod.7b01012
J. Nat. Prod. 2018, 81, 703−721

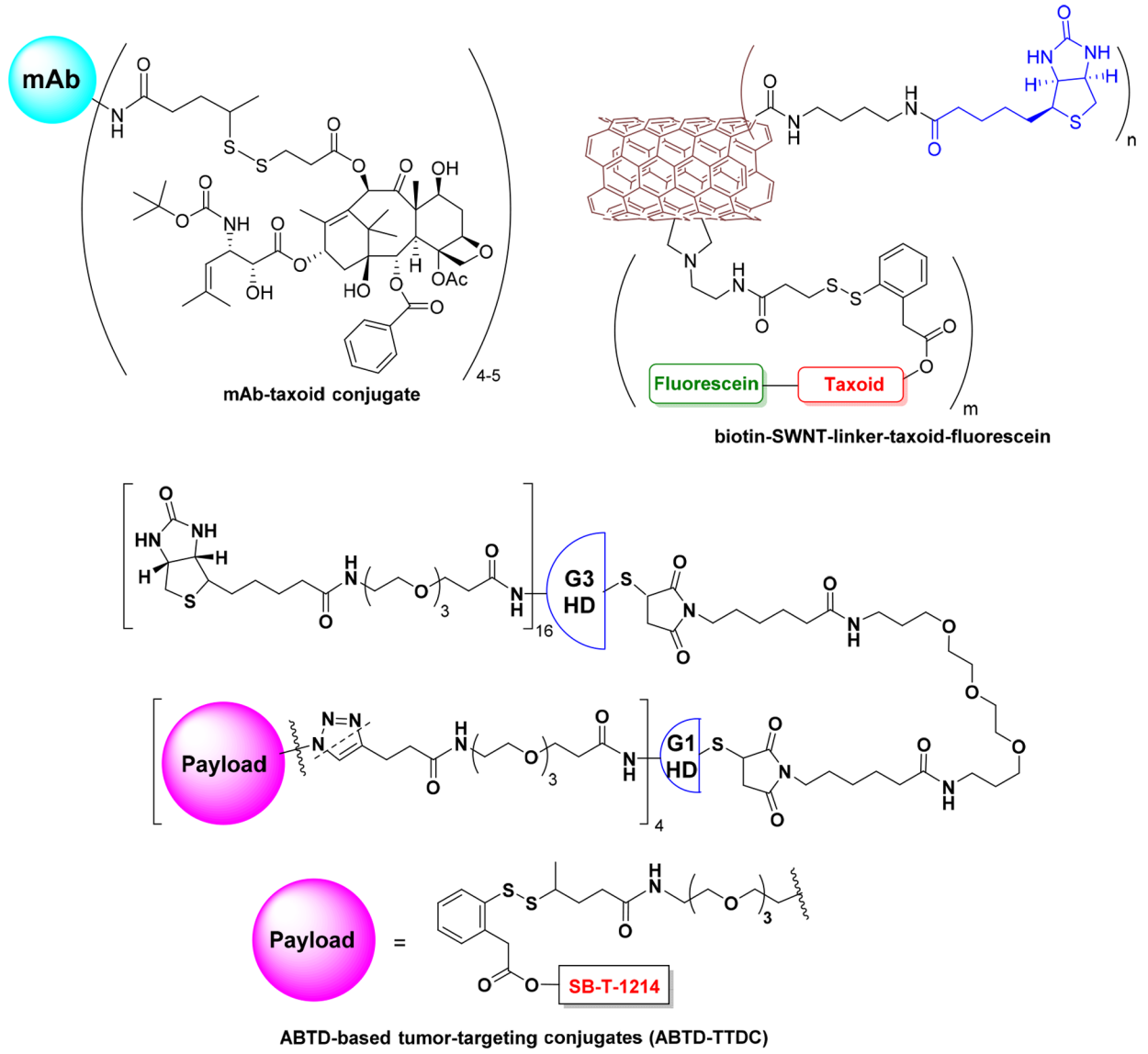

Figure 22. Nanoscale tumor-targeting drug delivery systems (1).

solved the oxygen sensitivity issue and proved very stable at 4–6 °C for a long period of time.[137] NE-DHA-SB-T-1214 exhibited remarkable in vivo efficacy against CSC-initiated PPT2 human prostate tumor xenografts in SCID mice, inducing tumor regression.[137] In the same experiment, Abraxane was not able to control the tumor growth of CSC-PPT2. Viable cells that survived this treatment regimen in vivo were no longer able to induce floating spheroids and holoclones, whereas control and Abraxane-treated tumor cells induced a large number of both. In addition, any complication in histopathology of different mouse organs was observed and also there is no significant weight change over the period of the treatment regimen.[137] NE-DHA-SB-T-1214 is currently in a late stage preclinical development for IND filing, which will be done in the near future.

CONCLUSIONS

This account has summarized our approaches to the successful discovery and development of highly potent next-generation taxoids based on SAR and systematic and logical drug design. These highly potent taxoids, however, will not be useful as single agents for cancer chemotherapy, but should be very promising for use as payloads for tumor-targeted drug delivery systems, as well as for combination therapies. We have described here an interesting history of a common pharmacophore concept and proposal for several naturally occurring microtubule-stabilizing anticancer agents. We witnessed the tricky nature of protein models in crystallography and the importance of the use of native proteins for the determination of protein-bound drug structures. Analyses of the protein-bound paclitaxel structure models through solid-state NMR studies and computational analysis have led to the design and synthesis of excellent paclitaxel mimics with very good synthetic challenges. We have found that the next-generation taxoids can promote rapid tubulin polymerization and produce numerous shorter microtubules. The analysis of thermodynamic parameters has revealed that the protein-binding process of the next-generation taxoids should be very different from that of paclitaxel. Some of the next-generation taxoids possess excellent activity against CSCs and tumors initiated by CSCs in vivo. This activity was found to be attributed to the ability of these taxoids to suppress "stemness genes" and promote cell

DOI: 10.1021/acs.jnatprod.7b01012
J. Nat. Prod. 2018, 81, 703–721

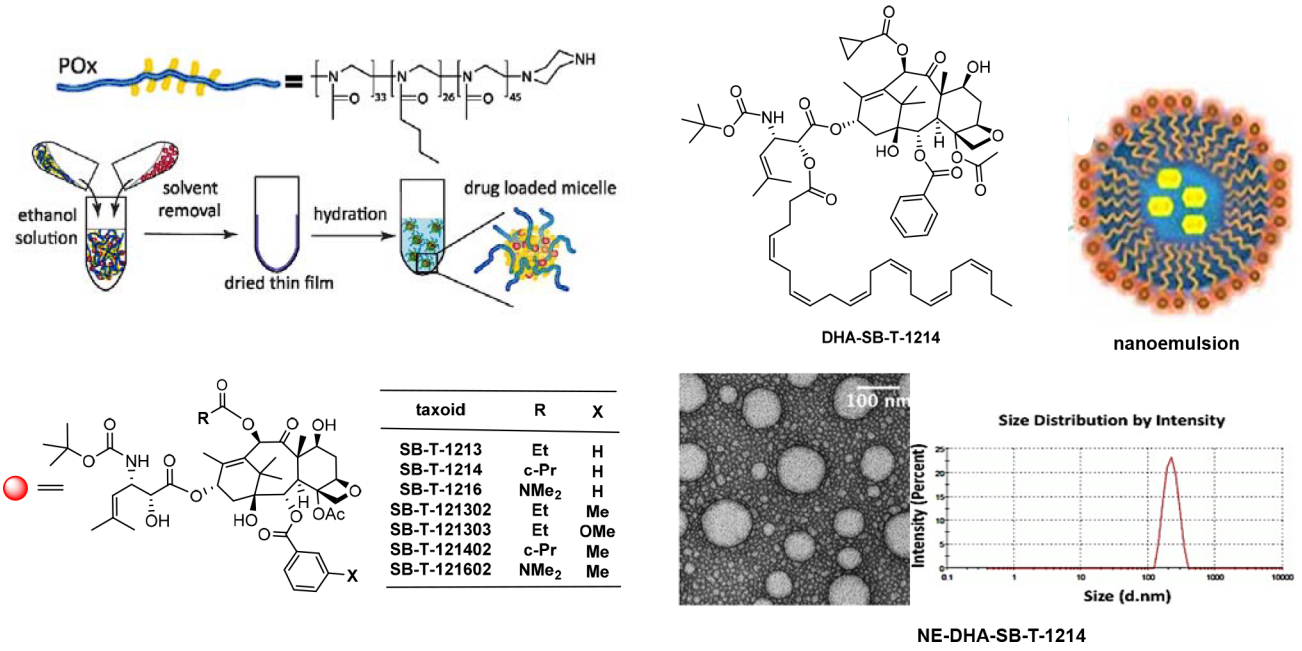

Figure 23. Nanoscale tumor-targeting drug delivery systems (2). Adapted from refs 134 and 137 with permission.

differentiation. Also, next-generation taxoids have been found to have an ability to block invasion and metastasis, as well as epithelial−mesenchymal transition. Finally, we have described the development of efficacious tumor-targeted drug delivery of taxoids based on tumor-targeting drug conjugates as small molecules as well as macromolecules/nanoparticles, including nanoemulsion formulations, which have a bright prospect for clinical applications.

AUTHOR INFORMATION

Corresponding Author

*E-mail: iwao.ojima@stonybrook.edu. Tel: +1 (631) 632-1339. Fax: +1 (631) 632-7942.

ORCID

Iwao Ojima: 0000-0002-3628-1161

Notes

The authors declare no competing financial interest.

ACKNOWLEDGMENTS

This research was supported by a grant from the National Institute of Health (CA 103314 to I.O.). Generous support from Indena SpA is gratefully acknowledged.

DEDICATION

Dedicated to Dr. Susan Band Horwitz, of Albert Einstein College of Medicine, Bronx, NY, for her pioneering work on bioactive natural products.

REFERENCES

(1) Murray, S.; Briasoulis, E.; Linardou, H.; Bafaloukos, D.; Papadimitriou, C. *Cancer Treat. Rev.* **2012**, *38*, 890−903.

(2) Rowinsky, E. K. *Annu. Rev. Med.* **1997**, *48*, 353−374.

(3) Bono, J. D.; Oudard, S.; Ozguroglu, M.; Hansen, S.; Machiels, J.; Shen, L.; Matthews, P.; Sartor, A. *J. Clin. Oncol.* **2010**, *28*, s4508.

(4) Georg, G. I.; Boge, T. C.; Cheruvallath, Z. S.; Clowers, J. S.; Harriman, G. C. B.; Hepperle, M.; Park, H. In *Taxol®: Science and Applications*; Suffness, M., Ed.; CRC Press: New York, 1995; pp 317−375.

(5) Georg, G. I.; Harriman, G. C. B.; Vander Velde, D. G.; Boge, T. C.; Cheruvallath, Z. S.; Datta, A.; Hepperle, M.; Park, H.; Himes, R. H.; Jayasinghe, L. In *Taxane Anticancer Agents: Basic Science and Current Status, ACS Symp. Series 583*; Georg, G. I.; Chen, T. T.; Ojima, I.; Vyas, D. M., Eds.; American Chemical Society: Washington, D.C., 1995; pp 217−232.

(6) Nicolaou, K. C.; Dai, W.-M.; Guy, R. K. *Angew. Chem., Int. Ed. Engl.* **1994**, *33*, 15−44.

(7) Kingston, D. G. I. *J. Nat. Prod.* **2000**, *63*, 726−734.

(8) Chauvière, G.; Guénard, D.; Picot, F.; Sénilh, V.; Potier, P. C. R. *Seances Acad. Sci., Ser. 2* **1981**, *293*, 501−503.

(9) Senilh, V.; Guéritte, F.; Guénard, D.; Colin, M.; Potier, P. C. R. *Séances Acad. Sci., Ser. 2* **1984**, *299*, 1039−1043.

(10) Parness, J.; Kingston, D. G. I.; Powell, R. G.; Harracksingh, C.; Horwitz, S. B. *Biochem. Biophys. Res. Commun.* **1982**, *105*, 1082−1089.

(11) Mellado, W.; Magri, N. F.; Kingston, D. G. I.; Garcia-Arenas, R.; Orr, G. A.; Horwitz, S. B. *Biochem. Biophys. Res. Commun.* **1984**, *124*, 329−336.

(12) Potier, P. *Chem. Soc. Rev.* **1992**, *21*, 113−119.

(13) Guenard, D.; Gueritte-Voegelein, F.; Potier, P. *Acc. Chem. Res.* **1993**, *26*, 160−167.

(14) Ojima, I. H. I.; Zhao, M.; Georg, G. I.; Jayasinghe, R. J. *J. Org. Chem.* **1991**, *56*, 1681−1684.

(15) Ojima, I. *Acc. Chem. Res.* **1995**, *28*, 383−389 and references therein.

(16) Ojima, I.; Habus, I.; Zhao, M.; Zucco, M.; Park, Y. H.; Sun, C. M.; Brigaud, T. *Tetrahedron* **1992**, *48*, 6985−7012.

(17) Ojima, I.; Sun, C. M.; Zucco, M.; Park, Y. H.; Duclos, O.; Kuduk, S. D. *Tetrahedron Lett.* **1993**, *34*, 4149−4152.

(18) Holton, R. A. U.S. Pat. 5175315, 1992

(19) Holton, R. A.; Biediger, R. J.; Boatman, P. D., In *Taxol: Science and Applications*; Suffness, M., Ed.; CRC Press: Boca Raton, 1995; pp 97−121.

(20) Ojima, I.; Kuduk, S. D.; Chakravarty, S., In *Advances in Medicinal Chemistry*, Maryanoff, B. E.; Reitz, A. B., Eds.; JAI Press: Greenwich, CT, 1998; Vol. *4*, pp 69−124.

(21) Ojima, I.; Slater, J. C.; Michaud, E.; Kuduk, S. D.; Bounaud, P.-Y.; Vrignaud, P.; Bissery, M. C.; Veith, J. M.; Pera, P.; Bernacki, R. J. *J. Med. Chem.* **1996**, *39*, 3889−3896.

(22) Ojima, I.; Chen, J.; Sun, L.; Borella, C. P.; Wang, T.; Miller, M. L.; Lin, S. N.; Geng, X. D.; Kuznetsova, L. R.; Qu, C. X.; Gallager, D.; Zhao, X. R.; Zanardi, I.; Xia, S. J.; Horwitz, S. B.; Mallen-St Clair, J.;

DOI: 10.1021/acs.jnatprod.7b01012
J. Nat. Prod. 2018, 81, 703−721

Guerriero, J. L.; Bar-Sagi, D.; Veith, J. M.; Pera, P.; Bernacki, R. J. *J. Med. Chem.* **2008**, *51*, 3203−3221.
(23) Chaudhary, A. G.; Gharpure, M. M.; Rimoldi, J. M.; Chordia, M. D.; Gunatilaka, A. A. L.; Kingston, D. G. I.; Grover, S.; Lin, C. M.; Hamel, E. *J. Am. Chem. Soc.* **1994**, *116*, 4097−4098.
(24) Kingston, D. G. I.; Chaudhary, A. g.; Chordia, M. D.; Gharpure, M.; Gunatilaka, A. A. L.; Higgs, P. I.; Rimoldi, J. M.; Samala, L.; Jagtap, P. G.; Giannakakou, P.; Jiang, Y. Q.; Lin, C. M.; Hamel, E.; Long, B. H.; Fairchild, C. R.; Johnston, K. A. *J. Med. Chem.* **1998**, *41*, 3715−3726.
(25) Ojima, I.; Wang, T.; Miller, M. L.; Lin, S.; Bollera, C. P.; Geng, X.; Pera, P.; Bernacki, R. J. *Bioorg. Med. Chem. Lett.* **1999**, *9*, 3423−3428.
(26) Ojima, I.; Lin, S.; Wang, T. *Curr. Med. Chem.* **1999**, *6*, 927−954.
(27) Ojima, I.; Das, M. *J. Nat. Prod.* **2009**, *72*, 554−565.
(28) Matesanz, R.; Trigili, C.; Rodriguez-Salarichs, J.; Zanardi, I.; Pera, B.; Nogales, A.; Fang, W. S.; Jimenez-Barbero, J.; Canales, A.; Barasoain, I.; Ojima, I.; Diaz, J. F. *Bioorg. Med. Chem.* **2014**, *22*, 5078−5090.
(29) Appendino, G.; Gariboldi, P.; Gabetta, B.; Pace, R.; Bombardelli, E.; Viterbo, D. *J. Chem. Soc., Perkin Trans. 1* **1992**, *1*, 2925−2929.
(30) Ojima, I.; Park, Y. H.; Sun, C.-M.; Fenoglio, I.; Appendino, G.; Pera, P.; Bernacki, R. J. *J. Med. Chem.* **1994**, *37*, 1408−1410.
(31) Ojima, I.; Slater, J. C.; Kuduk, S. D.; Takeuchi, C. S.; Gimi, R. H.; Sun, C.-M.; Park, Y. H.; Pera, P.; Veith, J. M.; Bernacki, R. J. *J. Med. Chem.* **1997**, *40*, 267−278.
(32) http://www.sppirx.com/335-spectrum-products-development-ortataxel.html.
(33) Ferlini, C.; Raspaglio, G.; Mozzetti, S.; Cicchillitti, L.; Filippetti, F.; Gallo, D.; Fattorusso, C.; Campiani, G.; Scambia, G. *Cancer Res.* **2005**, *65*, 2397−2405.
(34) Pepe, A.; Sun, L.; Zanardi, I.; Wu, X.; Ferlini, C.; Fontana, G.; Bombardelli, E.; Ojima, I. *Bioorg. Med. Chem. Lett.* **2009**, *19*, 3300−3304.
(35) Ojima, I.; Lin, S.; Slater, J. C.; Wang, T.; Pera, P.; Bernacki, R. J.; Ferlini, C.; Scambia, G. *Bioorg. Med. Chem.* **2000**, *8*, 1619−1628.
(36) Kuznetsova, L. V.; Ungureanu, I. M.; Pepe, A.; Zanardi, I.; Wu, X.; Ojima, I. *J. Fluorine Chem.* **2004**, *125*, 487−500.
(37) Kuznetsova, L. V.; Pepe, A.; Ungureanu, I. M.; Pera, P.; Bernacki, R. J.; Ojima, I. *J. Fluorine Chem.* **2008**, *129*, 817−828.
(38) Gut, I.; Ojima, I.; Vaclavikova, R.; Simek, P.; Horsky, S.; Linhart, I.; Soucek, P.; Kondrova, E.; Kuznetsova, L. V.; Chen, J. *Xenobiotica* **2006**, *36*, 772−92.
(39) Kuznetsova, L.; Sun, L.; Chen, J.; Zhao, X. R.; Seitz, J.; Das, M.; Li, Y.; Veith, J. M.; Pera, P.; Bernacki, R. J.; Xia, S. J.; Horwitz, S. B.; Ojima, I. *J. Fluorine Chem.* **2012**, *143*, 177−188.
(40) Vobořilová, J.; Němcová, V.; Neubauerová, J.; Ojima, I.; Zanardi, I.; Gut, I.; Kovář, J. *Invest. New Drugs* **2011**, *29*, 411−423.
(41) Schiff, P.; Horwitz, S. B. *Proc. Natl. Acad. Sci. U. S. A.* **1980**, *77*, 1561−1565.
(42) Bollag, D. M.; McQueney, P. A.; Zhu, J.; Hensens, O.; Koupal, L.; Liesch, J.; Goetz, M.; Lazarides, E.; Woods, C. M. *Cancer Res.* **1995**, *55*, 2325−2333.
(43) Lindel, T.; Jensen, P. R.; Fenical, W.; Long, B. H.; Casazza, A. M.; Carboni, J.; Fairchild, C. R. *J. Am. Chem. Soc.* **1997**, *119*, 8744−8745.
(44) ter Haar, E.; Kowalski, R. J.; Hamel, E.; Lin, C. M.; Longley, R. E.; Gunasekera, S. P.; Rosenkranz, H. S.; Day, B. W. *Biochemistry* **1996**, *35*, 243−250.
(45) Tanaka, J.-i.; Higa, T. *Tetrahedron Lett.* **1996**, *37*, 5535−5538.
(46) Schiff, P. B.; Fant, J.; Horwitz, S. B. *Nature* **1979**, *277*, 665−667.
(47) Kowalski, R. J.; Giannakakou, P.; Gunasekera, S. P.; Longley, R. E.; Day, B. W.; Hamel, E. *Mol. Pharmacol.* **1997**, *52*, 613−622.
(48) Kowalski, R. J.; Giannakakou, P.; Hamel, E. *J. Biol. Chem.* **1997**, *272*, 2534−2541.
(49) Giannakakou, P.; Sackett, D. L.; Kang, Y.-K.; Zhan, Z.; Buters, J. T.; Fojo, T.; Poruchynsky, M. S. *J. Biol. Chem.* **1997**, *272*, 17118−17125.
(50) Ojima, I.; Chakravarty, S.; Inoue, T.; Lin, S.; He, L.; Horwitz, S. B.; Kuduk, S. D.; Danishefsky, S. J. *Proc. Natl. Acad. Sci. U. S. A.* **1999**, *96*, 4256−4261.
(51) Kowalski, R.; Terhaar, E.; Longley, R.; Gunasekera, S.; Lin, C.; Day, B.; Hamel, E. In *Comparison of Novel Microtubule Polymerizing Agents, Discodermolide and Epothilone A/B, with Taxol*; Molecular Biology of the Cell 1995; Amer. Soc. Cell Biol. Publ. Office, 1995; pp 2137−2137.
(52) Hung, D. T.; Chen, J.; Schreiber, S. L. *Chem. Biol.* **1996**, *3*, 287−293.
(53) Gueritte-Voegelein, F.; Guenard, D.; Mangatal, L.; Potier, P.; Guilhem, J.; Cesario, M.; Pascard, C. *Acta Crystallogr., Sect. C: Cryst. Struct. Commun.* **1990**, *46*, 781−784.
(54) Mastropaolo, D.; Camerman, A.; Luo, Y.; Brayer, G. D.; Camerman, N. *Proc. Natl. Acad. Sci. U. S. A.* **1995**, *92*, 6920−6924.
(55) Ojima, I.; Kuduk, S. D.; Chakravarty, S.; Ourevitch, M.; Begue, J. P. *J. Am. Chem. Soc.* **1997**, *119*, 5519−5527.
(56) Ojima, I.; Lin, S.; Inoue, T.; Miller, M. L.; Borella, C. P.; Geng, X.; Walsh, J. J. *J. Am. Chem. Soc.* **2000**, *122*, 5343−5353.
(57) Nogales, E.; Wolf, S. G.; Downing, K. H. *Nature* **1998**, *391*, 199−203.
(58) Nettles, J. H.; Li, H.; Cornett, B.; Krahn, J. M.; Snyder, J. P.; Downing, K. H. *Science* **2004**, *305*, 866−869.
(59) Reese, M.; Sánchez-Pedregal, V. M.; Kubicek, K.; Meiler, J.; Blommers, M. J.; Griesinger, C.; Carlomagno, T. *Angew. Chem.* **2007**, *119*, 1896−1900.
(60) Manetti, F.; Maccari, L.; Corelli, F.; Botta, M. *Curr. Top. Med. Chem.* **2004**, *4*, 203−217.
(61) Forli, S.; Manetti, F.; Altmann, K. H.; Botta, M. *ChemMedChem* **2010**, *5*, 35−40.
(62) Tanaka, J.; Higa, T. *Tetrahedron Lett.* **1996**, *37*, 5535−5538.
(63) Miller, J. H.; Singh, A. J.; Northcote, P. T. *Mar. Drugs* **2010**, *8* (4), 1059−1079.
(64) Prota, A. E.; Bargsten, K.; Zurwerra, D.; Field, J. J.; Díaz, J. F.; Altmann, K.-H.; Steinmetz, M. O. *Science* **2013**, *339*, 587−590.
(65) Rao, S.; Orr, G. A.; Chaudhary, A. G.; Kingston, D. G. I.; Horwitz, S. B. *J. Biol. Chem.* **1995**, *270*, 20235−20238.
(66) Rao, S.; Krauss, N. E.; Heerding, J. M.; Swindell, C. S.; Ringel, I.; Orr, G. A.; Horwitz, S. B. *J. Biol. Chem.* **1994**, *269*, 3132−3134.
(67) Rao, S.; He, L.; Chakravarty, S.; Ojima, I.; Orr, G. A.; Horwitz, S. B. *J. Biol. Chem.* **1999**, *274*, 37990−37994.
(68) Snyder, J. P.; Nettles, J. H.; Cornett, B.; Downing, K. H.; Nogales, E. *Proc. Natl. Acad. Sci. U. S. A.* **2001**, *98*, 5312−5316.
(69) Löwe, J.; Li, H.; Downing, K.; Nogales, E. *J. Mol. Biol.* **2001**, *313*, 1045−1057.
(70) Ojima, I.; Inoue, T.; Slater, J. C.; Lin, S.; Kuduk, S. D.; Chakravarty, S.; Walsh, J. J.; Cresteil, T.; Monsarrat, B.; Pera, P.; Bernacki, R. J. In *ACS Symp. Ser. 746: Asymmetric Fluoroorganic Chemistry*; Ramachandran, P. V., Ed.; American Chemical Society: Washington, D.C., 1999; Vol. *746*, pp 158−181.
(71) Li, Y. K.; Poliks, B.; Cegelski, L.; Poliks, M.; Gryczynski, Z.; Piszczek, G.; Jagtap, P. G.; Studelska, D. R.; Kingston, D. G. I.; Schaefer, J.; Bane, S. *Biochemistry* **2000**, *39*, 281−291.
(72) Paik, Y.; Yang, C.; Metaferia, B.; Tang, S.; Bane, S.; Ravindra, R.; Shanker, N.; Alcaraz, A. A.; Johnson, S. A.; Schaefer, J.; O'Connor, R. D.; Cegelski, L.; Snyder, J. P.; Kingston, D. G. I. *J. Am. Chem. Soc.* **2007**, *129*, 361−370.
(73) Geney, R.; Sun, L.; Pera, P.; Bernacki, R. J.; Xia, S.; Horwitz, S. B.; Simmerling, C. L.; Ojima, I. *Chem. Biol.* **2005**, *12*, 339−348.
(74) Williams, H. J.; Moyna, G.; Scott, A. I.; Swindell, C. S.; Chirlian, L. E.; Heerding, J. M.; Williams, D. K. *J. Med. Chem.* **1996**, *39*, 1555−1559.
(75) Sun, L.; Simmerling, C.; Ojima, I. *ChemMedChem* **2009**, *4*, 719−731.
(76) Ganesh, T.; Guza, R. C.; Bane, S.; Ravindra, R.; Shanker, N.; Lakdawala, A. S.; Snyder, J. P.; Kingston, D. G. I. *Proc. Natl. Acad. Sci. U. S. A.* **2004**, *101*, 10006−10011.
(77) Ganesh, T.; Yang, C.; Norris, A.; Glass, T.; Bane, S.; Ravindra, R.; Banerjee, A.; Metaferia, B.; Thomas, S. L.; Giannakakou, P.;

DOI: 10.1021/acs.jnatprod.7b01012
J. Nat. Prod. 2018, 81, 703−721

Alcaraz, A. A.; Lakdawala, A. S.; Snyder, J. P.; Kingston, D. G. I. *J. Med. Chem.* **2007**, *50*, 713−725.
(78) Shanker, N.; Kingston, D. G. I.; Ganesh, T.; Yang, C.; Alcaraz, A. A.; Geballe, M. T.; Banerjee, A.; McGee, D.; Snyder, J. P.; Bane, S. *Biochemistry* **2007**, *46*, 11514−11527.
(79) Snyder, J. P.; Nevins, N.; Cicero, D. O.; Jansen, J. *J. Am. Chem. Soc.* **2000**, *122*, 724−725.
(80) Sun, L.; Geng, X.; Geney, R.; Li, Y.; Simmerling, C.; Li, Z.; Lauher, J. W.; Xia, S.; Horwitz, S. B.; Veith, J. M.; Pera, P.; Bernacki, R. J.; Ojima, I. *J. Org. Chem.* **2008**, *73*, 9584−9593.
(81) Gunasekera, S. P.; Gunasekera, M.; Longley, R. E.; Schulte, G. K. *J. Org. Chem.* **1990**, *55*, 4912−4915.
(82) Gunasekera, S. P.; Gunasekera, M.; Longley, R. E.; Schulte, G. K. *J. Org. Chem.* **1991**, *56*, 1346.
(83) Klein, L. E.; Freeze, B. S.; Smith, A. B., III; Horwitz, S. B. *Cell Cycle* **2005**, *41*, 501−507.
(84) Jordan, M. A.; Ojima, I.; Rosas, F.; Distefano, M.; Wilson, L.; Scambia, G.; Ferlini, C. *Chem. Biol.* **2002**, *9*, 93−101.
(85) Dalerba, P.; Cho, R. W.; Clarke, M. F. *Annu. Rev. Med.* **2007**, *58*, 267−284.
(86) Reya, T.; Morrison, S. J.; Clarke, M. F.; Weissman, I. L. *Nature* **2001**, *414*, 105−111.
(87) Botchkina, G. I.; Zuniga, E. S.; Das, M.; Wang, Y.; Wang, H.; Zhu, S.; Savitt, A. G.; Rowehl, R. A.; Leyfman, Y.; Ju, J.; Shroyer, K.; Ojima, I. *Mol. Cancer* **2010**, *9*, 192.
(88) Botchkina, G. I.; Zuniga, E. S.; Rowehl, R. H.; Park, R.; Bhalla, R.; Bialkowska, A. B.; Johnson, F.; Golub, L. M.; Zhang, Y.; Ojima, I.; Shroyer, K. R. *PLoS One* **2013**, *8*, e69884.
(89) Zuniga, E. S. Design, synthesis and biological evaluation of new-generation taxoid-based tumor-targeting drug conjugates. Ph.D. dissertation; Stony Brook University, 2012.
(90) Li, F.; Tiede, B.; Massague, J.; Kang, Y. *Cell Res.* **2007**, *17*, 3−14.
(91) Jelínek, M.; Balušíková, K.; Fidlerová, J.; Němcová-Fürstová, V.; Kopperová, D.; Šrámek, J.; Zanardi, I.; Ojima, I.; Kovář, J. *Cancer Cell Int.* **2013**, *13*, 42.
(92) Ojima, I.; Kumar, K.; Awasthi, D.; Vineberg, J. G. *Bioorg. Med. Chem.* **2014**, *22*, 5060−5077.
(93) Jelinek, M.; Kabelova, A.; Sramek, J.; Seitz, J.; Ojima, I.; Kovar, J. *Anticancer Res.* **2017**, *37*, 1581−1590.
(94) Witkiewicz, A. K.; McMillan, E. A.; Balaji, U.; Baek, G.; Lin, W. C.; Mansour, J.; Mollaee, M.; Wagner, K. U.; Koduru, P.; Yopp, A.; Choti, M. A.; Yeo, C. J.; McCue, P.; White, M. A.; Knudsen, E. S. *Nat. Commun.* **2015**, *6*, 6744.
(95) Mohelnikova-Duchonova, B.; Kocik, M.; Duchonova, B.; Brynychova, V.; Oliverius, M.; Hlavsa, J.; Honsova, E.; Mazanec, J.; Kala, Z.; Ojima, I.; Hughes, D. J.; Doherty, J. E.; Murray, H. A.; Crockard, M. A.; Lemstrova, R.; Soucek, P. *Pharmacogenomics J.* **2017**, *17*, 452−460.
(96) Zheng, X.; Wang, C.; Xing, Y.; Chen, S.; Meng, T.; You, H.; Ojima, I.; Dong, Y. *Int. J. Oncol.* **2017**, *50*, 893−902.
(97) Jaracz, S.; Chen, J.; Kuznetsova, L. V.; Ojima, I. *Bioorg. Med. Chem.* **2005**, *13*, 5043−5054.
(98) Koshkaryev, A.; Sawant, R.; Deshpande, M.; Torchilin, V. *Adv. Drug Delivery Rev.* **2013**, *65*, 24−35.
(99) Nagy, J. A.; Chang, S. H.; Dvorak, A. M.; Dvorak, H. F. *Br. J. Cancer* **2009**, *100*, 865−869.
(100) Maeda, H. *Adv. Enzyme Regul.* **2001**, *41*, 189−207.
(101) Farokhzad, O. C.; Cheng, J.; Teply, B. A.; Sherifi, I.; Jon, S.; Kantoff, P. W.; Richie, J. P.; Langer, R. *Proc. Natl. Acad. Sci. U. S. A.* **2006**, *103*, 6315−6320.
(102) Ducry, L.; Stump, B. *Bioconjugate Chem.* **2010**, *21*, 5−13.
(103) Xia, W.; Low, P. S. *J. Med. Chem.* **2010**, *53*, 6811−6824.
(104) Ojima, I.; Zuniga, E. S.; Berger, W. T.; Seitz, J. D. *Future Med. Chem.* **2012**, *4*, 33−50.
(105) Ojima, I. *ChemBioChem* **2004**, *5*, 628−635.
(106) Carter, P. J.; Senter, P. D. *Cancer J.* **2008**, *14*, 154−169.
(107) Zolot, R. S.; Basu, S.; Million, R. P. *Nat. Rev. Drug Discovery* **2013**, *12*, 259−260.
(108) Ojima, I.; Geng, X. D.; Wu, X. Y.; Qu, C. X.; Borella, C. P.; Xie, H. S.; Wilhelm, S. D.; Leece, B. A.; Bartle, L. M.; Goldmacher, V. S.; Chari, R. V. J. *J. Med. Chem.* **2002**, *45*, 5620−5623.
(109) Chen, J.; Jaracz, S.; Zhao, X.; Chen, S.; Ojima, I. *Expert Opin. Drug Delivery* **2005**, *2*, 873−890.
(110) Chari, R. V. J.; Miller, M. L.; Widdison, W. C. *Angew. Chem., Int. Ed.* **2014**, *53*, 3796−3827.
(111) Leamon, C. P. *Curr. Opin. Invest. Drugs* **2008**, *9*, 1277−1286.
(112) Vlahov, I. R.; Leamon, C. P. *Bioconjugate Chem.* **2012**, *23*, 1357−1369.
(113) Vlahov, I. R.; Santhapuram, H. K.; Kleindl, P. J.; Howard, S. J.; Stanford, K. M.; Leamon, C. P. *Bioorg. Med. Chem. Lett.* **2006**, *16*, 5093−5096.
(114) Chen, S.; Zhao, X.; Chen, J.; Chen, J.; Kuznetsova, L.; Wong, S. S.; Ojima, I. *Bioconjugate Chem.* **2010**, *21*, 979−987.
(115) Vineberg, J. G.; Zuniga, E. S.; Kamath, A.; Chen, Y.-J.; Seitz, J. D.; Ojima, I. *J. Med. Chem.* **2014**, *57*, 5777−5791.
(116) Warnecke, A. In *Drug Delivery in Oncology: From Basic Research to Cancer Therapy*; Kratz, F.; Peter Senter, P.; Steinhagen, H., Eds.; Wiley-VCH: Weinheim, 2011; Vol. *2*, pp 553−589.
(117) Ojima, I. *Acc. Chem. Res.* **2008**, *41*, 108−119.
(118) Chen, J.; Chen, S.; Zhao, X.; Kuznetsova, L. V.; Wong, S. S.; Ojima, I. *J. Am. Chem. Soc.* **2008**, *130*, 16778−16885.
(119) Vineberg, J. G.; Wang, T.; Zuniga, E. S.; Ojima, I. *J. Med. Chem.* **2015**, *58*, 2406−2416.
(120) Crider, K. S.; Yang, T. P.; Berry, R. J.; Bailey, L. B. *Adv. Nutr.* **2012**, *3*, 21−38.
(121) Hassan, Y. I.; Zempleni, J. *J. Nutr.* **2006**, *136*, 1763−1765.
(122) Wakil, S. J. *J. Lipid Res.* **1961**, *2*, 1−24.
(123) Russell-Jones, G.; McTavish, K.; McEwan, J.; Rice, J.; Nowotnik, D. *J. Inorg. Biochem.* **2004**, *98*, 1625−1633.
(124) Vineberg, J. G. Design, synthesis, and biological evaluation of novel taxoid-based drug conjugates and theranostic imaging agents towards tumor-targeted chemotherapy. Ph.D. dissertation; Stony Brook University, 2014.
(125) Kigawa, J.; Minagawa, Y.; Kanamori, Y.; Itamochi, H.; Cheng, X.; Okada, M.; Oisho, T.; Terakawa, N. *Cancer* **1998**, *82*, 697−702.
(126) Zheng, Z. B.; Zhu, G.; Tak, H.; Joseph, E.; Eiseman, J. L.; Creighton, D. J. *Bioconjugate Chem.* **2005**, *16*, 598−607.
(127) Seitz, J. D.; Vineberg, J. G.; Wei, L.; Khan, J. F.; Lichtenthal, B.; Lin, C.-F.; Ojima, I. *J. Fluorine Chem.* **2015**, *171*, 148−161.
(128) Seitz, J. D.; Vineberg, J. G.; Herlihy, E.; Park, B.; Melief, E.; Ojima, I. *Bioorg. Med. Chem.* **2015**, *23*, 2187−2194.
(129) Seitz, J. D. The design, synthesis and biological evaluation of novel taxoid anticancer agents and their tumor-targeted drug conjugates. Ph.D. disseration; Stony Brook University, 2013.
(130) Chari, R. V. *Adv. Drug Delivery Rev.* **1998**, *31*, 89−104.
(131) Beck, A.; Haeuw, J. F.; Wurch, T.; Goetsch, L.; Bailly, C.; Corvaia, N. *Discovery Med.* **2010**, *10*, 329−339.
(132) Verma, S.; Miles, D.; Gianni, L.; Krop, I. E.; Welslau, M.; Baselga, J.; Pegram, M.; Oh, D. Y.; Dieras, V.; Guardino, E.; Fang, L.; Lu, M. W.; Olsen, S.; Blackwell, K.; Grp, E. S. *N. Engl. J. Med.* **2012**, *367*, 1783−1791.
(133) Ojima, I.; Wang, T.; Teng, Y.-H. G. Asymmetric Bow-Tie Dendrimers as Versatile Platform for Drug Delivery and Diagnosis. WO 2015038493 A1, 2015.
(134) He, Z.; Schulz, A.; Wan, X.; Seitz, J.; Bludau, H.; Alakhova, D. Y.; Darr, D. B.; Perou, C. M.; Jordan, R.; Ojima, I.; Kabanov, A. V.; Luxenhofer, R. *J. Controlled Release* **2015**, *208*, 67−75.
(135) Seitz, J. D.; Ojima, I. In *Drug Delivery in Oncology - From Research Concepts to Cancer Therapy*; Kratz, F.; Senter, P.; Steinhagen, H., Eds.; Wiley-VCH: Weinheim, 2011; Vol. *3*, pp 1323−1360.
(136) Kuznetsova, L.; Chen, J.; Sun, L.; Wu, X.; Pepe, A.; Veith, J. M.; Pera, P.; Bernacki, R. J.; Ojima, I. *Bioorg. Med. Chem. Lett.* **2006**, *16*, 974−977.
(137) Ahmad, G.; El Sadda, R.; Botchkina, G.; Ojima, I.; Egan, J.; Amiji, M. *Cancer Lett.* **2017**, *406*, 71−80.

DOI: 10.1021/acs.jnatprod.7b01012
J. Nat. Prod. 2018, 81, 703−721